Draft Note.

Renormalization of group field theories for quantum gravity: new scaling results and some suggestions

Marco Finocchiaro[a,c] **Daniele Oriti**[b]

[a] *Max Planck Institute for Gravitational Physics (Albert Einstein Institute), Am Muehlenberg 1, D-14476 Potsdam-Golm, Germany, EU*

[b] *Arnold-Sommerfeld-Center for Theoretical Physics, Ludwig-Maximilians-Universität, Theresienstrasse 37, D-80333 München, Germany, EU*

[c] *Institute for Physics, Humboldt-Universität zu Berlin, Newtonstraße 15, 12489 Berlin, Germany, EU*

E-mail: marco.finocchiaro@aei.mpg.de, daniele.oriti@physik.lmu.de

Abstract: We discuss motivation and goals of renormalization analyses of group field theory models of simplicial 4d quantum gravity, and review briefly the status of this research area. We present some new computations of perturbative GFT (spin foam) amplitudes, concerning in particular the scaling behaviour of radiative corrections to N-point functions. Finally, we single out key open issues and suggest a number of research directions for further progress in this area.

1 Introduction

Group field theories (GFT) [1–3] are quantum field theories which aim at describing the fundamental quantum structures that constitute spacetime. They are quantum field theories *of* spacetime, rather than *on* spacetime. They are defined on group manifolds (hence the name), with an associated phase space given by the cotangent bundle of the same group . Specifically, the typical GFT field is a tensor $\varphi(g_1, ..., g_d)$, mapping the direct product of d copies of a Lie group to the complex numbers:

$$\varphi : G^{\times d} \to \mathbb{C} .$$

Equivalently, in conjugate variables, the basic field maps d copies of the lie algebra of the same group to the complex numbers, and should be understood in general as a non-commutative function, since the Lie algebra is in general a non-commutative manifold. Depending on the specific model one is considering, various restriction can be imposed on the field, its domain, its target, and of course the choice of group manifold and 'dimension'd are also model-dependent. What is general, in all current GFT models, is that the basic quanta of the theory, corresponding to the basic field excitations, can be represented as abstract cells or polyhedra with the d algebraic data forming the domain of the field associated to their (boundary) faces. When d is chosen as the dimension of the spacetime to be reproduced in some approximation, the corresponding GFT quanta can be understood as $(d-1)$-simplices with algebraic labels on their d $(d-2)$-dimensional faces. This is the case we restrict to in the following. The other feature which constitutes another defining aspect of the formalism is the peculiar combinatorial structure of field interactions. The dynamics of the theory, which dictates how the fundamental GFT quanta interact forming extended spacetime structure, is specified by an action, first,

$$S(\varphi, \varphi^*) = \frac{1}{2}\int [dg]\, \varphi^*\, \mathcal{K}(g_i)\, \varphi(g_i) \; + \; \frac{\lambda}{n!}\int [dg_{ia}]\, \varphi(g_{i1})...\varphi(g_{in})\, \mathcal{V}(g_{ia}) \; + \; c.c.$$

and then by its partition function (assumed here as being of statistical form):

$$Z = \int \mathcal{D}\varphi \mathcal{D}\varphi^*\; e^{-\,S_\lambda(\varphi,\varphi^*)} .$$

Beside a quadratic local term, the GFT action is determined by interactions (just one in the above example) that possess a characteristic 'combinatorial non-locality'in that the interaction kernels pair non-locally the field arguments (d variables being contributed by each field entering the given interaction term). Interaction kernels of order n can be associated with possible ways of gluing together n $(d-1)$-simplices to form (the boundary of) a d-dimensional cell. The specific combinatorial patterns (i.e. the specific cells being associated to each fundamental interaction) and interaction kernels (as well as the kinetic term) are part of the definition of each GFT model. However, from this generic aspect of the formalism follows one key fact: GFT Feynman diagrams Γ generated by the perturbative expansion of the GFT partition function,

$$Z = \int \mathcal{D}\varphi \mathcal{D}\varphi^*\; e^{-\,S_\lambda(\varphi,\varphi^*)} \; = \; \sum_\Gamma \frac{\lambda^{N_\Gamma}}{sym(\Gamma)}\, \mathcal{A}_\Gamma$$

obtained gluing interaction vertices (d-cells) along their $(d-1)$-faces, are dual to d-dimensional cellular complexes, of arbitrary topology (since a priori there is no restriction on the allowed gluings). The Feynman amplitudes assign a probability amplitude for each such cellular complex, seen as an elementary interaction process of the fundamental GFT quanta.

1.1 GFT, spin foams and other quantum gravity formalisms

We recognize in this brief outline the straightforward generalization of how 2d surfaces are generated in the perturbative expansion of random matrix models. Indeed, GFTs can be seen as group-theoretic enrichment of random *tensor* models [4–6], to which they reduce if the Lie group domain is replaced by any finite set of N elements. The Feynman amplitudes become purely combinatorial, but the type of diagrams remains the same. Seen as tensors, GFT fields admit a natural action of unitary (and orthogonal) groups on their arguments. If one requires GFT interactions to be invariant under such unitary transformations, they can be fully classified, and we speak of *tensorial* GFT models. Most of the literature on GFT renormalization [7, 8] concerns these

tensorial GFT models. More generally, focusing on tensorial aspects of GFTs allows to gain a greater control over the combinatorial structures of their states, diagrams and amplitudes and many of the results obtained in the simpler context of tensor models apply also to GFTs: the use of colors to encode the topology of Feynman diagrams, the large-N expansion, double scaling limits, universality results etc. The first two, in particular, are crucial for GFT renormalization.

In this contribution, we focus on GFT models which are 'quantum geometric': their fundamental quanta are quantised tetrahedra with a quantum geometry encoded in group-theoretic data. More precisely, the classical phase space of a single Lorentzian tetrahedron in 4d is chosen to be the cotangent bundle of 4 copies $SL(2,\mathbb{C})$, reduced by additional 'geometricity'constraints, and in turn this can be mapped, under the same constraints, to the cotangent bundle of 4 copies of $SU(2)$. Appropriate gluing of five geometric tetrahedra on the boundary of a combinatorial 4-simplex can then be shown to provide a geometric characterization of the 4-simplex too, and of the whole simplicial complex obtained gluing geometric 4-simplices together. The same construction in the Riemannian case uses $Spin(4)$ instead of $SL(2,\mathbb{C})$. From the choice of classical phase space follows a choice of Hilbert space for individual quanta of the GFT model, given in one representation by $L^2(G^4)$ reduced by the quantum counterpart of the geometricity constraints, where G is one of the chosen groups mentioned above, while the complete Hilbert space is the corresponding Fock space built on this single-quantum Hilbert space. We will give a few more details in the next subsection.

For this class of geometric models, the GFT formalism benefits from direct links to other modern quantum gravity approaches, which can, viceversa, benefit from GFT tools and results.

First, of all, when $SU(2)$ is used, the Hilbert space of a single GFT quantum is the same as that of a loop quantum gravity (LQG) [9] 4-valent spin network vertex. Generic GFT states, organized in a Fock space, will be populated by many such vertices and they will include, in particular, states corresponding to spin networks associated to closed graphs and gauge-invariant cylindrical functions for the same graphs. In fact, the LQG Hilbert space associated to any graph can be shown to be faithfully embedded in the GFT Fock space. The theories however differ in the way these graph-based Hilbert spaces are related, more precisely, in the scalar products between states associated to different graphs. Still, the correspondence, which can be extended to observables and quantum dynamics, allows to see GFTs as a 2nd quantized counterpart of LQG [10].

Next. for this class of models, the GFT Feynman amplitudes take the form of (non-commutative) simplicial gravity path integrals [11, 12], when written in (non-commutative) Lie algebra variables, which encode the discrete metric. The group variables, on the other hand, are understood as encoding the discrete gravity connection. They correspond indeed to discretizations of a classical formulation of gravity as a topological BF theory with added geometricity constraints, on the simplicial complex dual to the GFT Feynman diagrams. The specific way in which the BF action is discretized depend on the quantization map applied to Lie algebra variables, and different models correspond to different strategies for the imposition of the constraints and path integral measures.

In fact, when the same Feynman amplitudes are recast as functions of group representations, using Peter-Weyl or Plancherel decomposition, they take the form of spin foam models [13]. Spin foam models have been introduced as a covariant language for computing spin network dynamics, so they can be understood as a covariant counterpart of canonical loop quantum gravity. A second perspective is to see spin foam amplitudes as a purely algebraic version of lattice gravity path integrals, or state sum models. In GFT, they arise as Feynman amplitudes. The correspondence is generic: for any given set of spin foam amplitudes associated to simplicial complexes (and admitting a local decomposition with respect to the complex), one can find a GFT action such that the perturbative expansion of the quantum partition function will produce the given amplitudes as Feynman amplitudes (and viceversa, any GFT action corresponds to a set of spin foam amplitudes). A complete definition of a spin foam model requires a prescription for the amplitudes to be associated to all possible cellular complexes (in some specified class) and an organization principle for them, i.e. one way of comparing, composing or selecting them, to obtain a single number for any observable one wants to compute. The GFT embedding provide one such clear organizing principle, by summing them in a QFT perturbative expansion. In addition, it provides a whole set of QFT tools that can be applied to study their mathematical foundations as well as for extracting physics. GFT renormalization can be seen, indeed, from this spin foam perspective.

1.2 Simplicial GFT models for 4d quantum gravity

The starting point for the construction of simplicial GFT (and spin foam) models of 4d quantum gravity is the quantum geometry of a single tetrahedron in 4d [14]. The quantum geometry of this basic building block, and the extended structured built from it, can be described in various parametrizations [15, 16], and a number of generalizations can also be defined [17, 18] and imported in the GFT framework. Classically, one can use two equivalent characterization of a tetrahedral geometry, leading immediately to an algebraic translation. First, one can start with assigning four vectors $b_i^I \in \mathbb{R}^{3,1}$ to the four faces of the tetrahedron, forced to lie all in the same spacelike hypersurface with timelike normal V (thus satisfying $b_i \cdot V = 0$), and thinking of them as normal to the same faces, with their modulus identified with their area, $b_i^I = A_i n_i^I$ (with $|n| = 1$). The vectors are also forced to close to form the closed boundary of the tetrahedron, i.e. $\sum_i b_i = 0$. The vectors b_i, due to the constraints they satisfy, are actually elements of the vector space $\mathbb{R}^3$ which can be identified with the Lie algebra $\mathfrak{su}(2)$, after it has been endowed with the corresponding Lie bracket. The resulting space $\mathfrak{su}(2)^{\times 4}$ is then the space of geometries for a single tetrahedron. It can also be seen as the cotangent space of the phase space $(\mathcal{T}^*SU(2))^{\times 4}$ which is then the phase space of a classical tetrahedron, purely expressed in terms of group-theoretic, algebraic data. The conjugate variables in $SU(2)^{\times 4}$ have the interpretation of parallel transports of a discrete connection along elementary paths from (the (bari)center of) the tetrahedron to the ((bari)center of its) boundary faces. The dual graph made of these paths becomes the graph associated to a single spin network vertex (with four outgoing 'open links'). In group representation, the corresponding Hilbert space is thus $L^2(SU(2)^4)$ (with Haar measure). An equivalent encoding of the classical geometry of a single tetrahedron uses directly the variables of discretized BF theory: all geometric quantities of a single tetrahedron can be computed starting from four bivectors $B_i^{IJ} \in \wedge^2\mathbb{R}^{3,1} \simeq \mathfrak{sl}(2,\mathbb{C})$ which close $\sum_i B_i^{IJ} = 0$ and satisfy the simplicity constraints $V_I(*B_i)^{IJ} = 0$ ($*$ is the hodge dual), with respect to the same timelike normal vector V. The phase space of a single tetrahedron can be taken to be the cotangent bundle $\mathcal{T}^*SL(2,\mathbb{C})^4$ and the Hilbert space to be $L^2(SL(2,\mathbb{C})^4)$. The two geometric descriptions can be mapped into each other. The simplicity constraints can be seen also, in fact, as determining such map [19]. Since the Hilbert spaces indicated above admit a basis labeled by group representations, this correspondence can be seen also at that level, i.e. as specifying how the relevant representations of $SL(2,\mathbb{C})$ should be decomposed in $SU(2)$ representations, if they have to be understood as encoding the quantum geometry of a tetrahedron. Such representation labels are the variables in which spin foam amplitudes are expressed. Different spin foam (and GFT) models for 4d quantum gravity are specified (among other things) by the way the impose the simplicity constraints at the quantum level, and thus by the specific map between $SL(2,\mathbb{C}$ and $SU(2)$ entering their amplitudes. In the Riemannian case, which will be our focus in this contribution, all the above applies, with $Spin(4)$ replacing $SL(2,\mathbb{C})$.

A spin foam amplitude, that is a GFT Feynman amplitude written in representation variables, will be assigned to any given simplicial complex, dual to a GFT Feynman diagram. The basic building block is an assignment of a quantum amplitude to each 4-simplex, i.e. a 'vertex'of the spin foam complex given by the GFT Feynman diagram, with this amplitude function of the algebraic data associated to the five tetrahedra on its boundary. These boundary data can be written as $SU(2)$ or $SL(2,\mathbb{C})$ data, using the mentioned map, and the vertex amplitude can be written as a function of both, featuring then the coefficients of the simplicity map in its expression. Thus the vertex amplitude will be a function of $SU(2)$ and $SL(2,\mathbb{C})$ representations associated to the triangles of the 4-simplex (faces of the dual complex), and intertwiners of both groups associated to the tetrahedra, following the imposition of the closure conditions (equivalent to gauge invariance with respect to both groups). The data not used as boundary data are then summed over independently in each vertex amplitude. The spin foam amplitude associated to the whole simplicial complex can then be obtained by gluing together the amplitudes associated to its 4-simplices, with the gluing amounting to matching first and then tracing over the data associated to the tetrahedron shared by each pair of 4-simplices, possibly weighted by an additional gluing kernel. In the GFT context, the vertex amplitude and the gluing kernel are nothing else than the interaction kernel and the propagator (inverse of the kinetic kernel) defining the GFT action.

The general formula for the spin foam amplitudes, for all the models in this class, in the Riemannian setting, for given cellular complex $\mathfrak{m}$ dual to the Feynman diagram Γ is the following:

$$\mathcal{A}^{\beta}(\mathfrak{m}) = \sum_{J_f j_{ef}} \sum_{I_{ve} i_e} \prod_{f\in\mathcal{F}_\mathfrak{m}} d_{J_f} \prod_{e\in f} d_{j_{ef}} \prod_{v\in\mathcal{V}_\mathfrak{m}} \{15J_f\}_v \prod_{e\in\mathcal{E}_\mathfrak{m}} d_{I_{ve}} \sqrt{d_{i_e}}\, f^{i_e,l/2}_{I_{ve}}(J_f, j_{ef}, k_e, \beta) \tag{1.1}$$

The coefficients f are matrix elements of the map between Spin(4) and SU(2) intertwiner spaces:

$$f^{i,l}_{I}(J_p, j_p, k, \beta) = \sum_{M_p m_p} (\mathcal{I})^{J_1 J_2 J_3 J_4 I}_{M_1 M_2 M_3 M_4} \left[\prod_{p=1}^{4} C^{j_p^- j_p^- j_p}_{m_p^- m_p^- m_p} (k) w^{l}(J_p, j_p, \beta) \right] (\mathcal{I})^{j_1 j_2 j_3 j_4 i}_{m_1 m_2 m_3 m_4} \tag{1.2}$$

where we have a Spin(4) representation J_f labelling each face, a pair of Spin(4) four-valent intertwiners I_{ve}, $I_{v'e}$ for every edge and an SO(3) spin j_{ef} for each edge in a given face. We have indicated with w the function of group representations that characterizes the simplicity map defining each model, depending on the representations of $Spin(4)$ and $SU(2)$ labelling each face of the complex. This depends also on the Immirzi parameter γ. The models we will deal with in the following are the EPRL model [13] and the Duflo BO model [12], whose defining maps are:

$$w_{EPRL}(j^-, j^+, j, \beta) = \delta_{j^- \,|\beta| j^+} \delta_{j\,(1+|\beta|)j^+} \quad \beta < 0 \qquad w_{EPRL}(j^-, j^+, j, \beta) = \delta_{j^- \,|\beta| j^+} \delta_{j\,(1-|\beta|)j^+} \quad \beta \geq 0 \tag{1.3}$$

$$w_{Duflo}(j^-, j^+, j, \beta) = \frac{(-1)^{j^- + j^+ + j}}{\pi \sqrt{(2j^- + 1)(2j^+ + 1)}} \sum_{a=0}^{\lambda} (\mathrm{Sign}(\beta))^a \begin{Bmatrix} a & j^- & j^- \\ j & j^+ & j^+ \end{Bmatrix} \mathcal{T}_a^{j^- j^+}(|\beta|) \tag{1.4}$$

We note that the relative simplicity/complexity of these two models is highly dependent on the basis in which they are expressed, with the flux representation switching such relative complexity with respect to the spin representation given above.

More details about the construction of spin foam amplitudes, in a language well adapted to their GFT embedding, can be found in [12].

2 Renormalization of group field theories for 4d quantum gravity

Let us now discuss motivation and current status of renormalization of simplicial GFT (and spin foam) models for quantum gravity.

Beyond the connection to spin foam models and simplicial gravity path integrals, the general strategy for renormalization of GFT models [7, 8, 20] is to treat them as ordinary QFTs defined on a Lie group manifold, thus using the group structures (topology, Killing forms, etc) to define 'scales'and mode integration. A natural notion of scale, to be used to label the RG flow, is provided by group representations, which index the spectrum of differential operators on the group, e.g. the Laplace-Beltrami operator, in turn often used to define the propagator of GFT models. Cut-offs imposed as part of a renormalization group scheme are then imposed on representation labels; for example, in the case of $SU(2)$ cutting off the spectrum of the Laplacian operator means imposing the bound $\sum_{i=1}^{d} j_i(j_i+1) \leq \Lambda^2$, for some real (large) number Λ. This fits well with the fact that divergences in spin foam amplitudes mostly come from the large representations regime. Still, a lot of non-trivial work (beside computational challenges) is needed to adapt for GFTs, whose Feynman diagrams are not graphs but cellular complexes, standard QFT notions, noticing also that any procedure for the contraction of divergent subgraphs of perturbative GFTs has the meaning, from the point of view of the simplicial gravity path integral or spin foam model corresponding to the Feynman amplitudes of the same, of a coarse graining scheme of the corresponding lattice theory.

For a proper renormalization group scheme, however, two more ingredients are needed: control over the theory space corresponding to a given GFT model, i.e. the space of allowed interactions; a detailed characterization of the combinatorics of (the cellular complexes dual to) GFT Feynman diagrams. On neither of these two points much is known for simplicial 4d gravity models. As a result, most work in the context of GFT renormalization has been done focusing on tensorial GFT models, where the above limitations are not present.

Before discussing the goals of GFT renormalization, we spend a few words of caution concerning the physical interpretation of the renormalization group scheme and derived flows. With scales associated to group

representation labels, the natural cutoffs entering as UV cutoffs are for large representations. The associated RG then flows from large to small representations (from UV to IR). In LQG and simplicial quantum geometry representation labels identify eigenvalues of geometric operators (e.g. triangle areas or tetrahedral volumes). Large representation labels correspond to large values of such geometric quantities. Thus we have an apparent inversion of roles here, with large distances/volumes playing the role of UV scales in GFT. Caution however should be exercised. In both LQG and simplicial geometry, we know an area of a surface, say, to result roughly speaking from the sum of the individual areas of all elementary surfaces forming the one under consideration, so that one has $A \approx < j >< N >$ with $< j >$ the average area contribution and $< N >$ the (average) number of contributions. Moreover, experience from classical Regge calculus and other simplicial gravity formalisms, leads us to expect continuum geometry to be reproduced when the number of elementary excitations contributing to a given continuum geometric quantity is very large, with each contribution smallish (but allowed to be orders of magnitude above Planck size). On the same basis, we expect continuum geometry, and with it any notion of large or small areas, volumes, distances etc, to be the result of coarse graining microscopic, fundamental degrees of freedom like the ones we deal with in the fundamental GFT (or spin foam) formalism. We would better refrain, then, from interpreting simplicial observables directly as geometric, in the sense we attribute to continuum spacetime geometry and physics. Finally, one more alert comes from recalling that, in GFT, the simplicial geometric observables and excitations are the ones associated to the Fock representation of the theory, and probably this is does not correspond to a fully geometric phase in which continuum gravitational (thus, spatiotemporal) physics is to be found, being best adapted to perturbation theory around the fully degenerate (from the point of view of geometry) Fock vacuum.

2.1 Quantum consistency and perturbative renormalization

GFT models are first defined in perturbative expansion and it is in this perturbative formulation that spin foam amplitudes, and simplicial gravity path integrals, appear. The perturbative GFT amplitudes generically diverge and regularizations have to be imposed. It is this truncation that corresponds to working at a given 'scale'. Is this definition of the quantum dynamics of GFT models consistent? is the spin foam description consistent? Here, consistency means first of all valid for all ranges of dynamical variables, under (controlled) removal of regulators. If not, the GFT model as defined in perturbative expansion, and thus the corresponding spin foam model (and simplicial path integral) cannot be trusted. In the GFT language, this is recognised immediately to be the issue of perturbative renormalizability of a given model. We should only trust, from the spin foam or lattice gravity point of view, only GFT models that turn out to be (perturbatively) renormalizable.

We note in passing that there should be no requirement that the model is finite; first, we have no obvious reason to expect it, if the model contains an infinite number of degrees of freedom; second, renormalizable models are usually more interesting, as QFTs, than finite ones, since they have a non-trivial RG flow and new effective physics at each scale.

Thus, the requirement of perturbative renormalizability is an important constraint, which helps removing from consideration inconsistent constructions. Here, the GFT embedding proves potentially very important also for spin foam models (and loop quantum gravity). All known GFT and spin foam models present several ambiguities, some intrinsic to any quantization procedure, others specific to simplicial GFT (and spin foam) models of quantum gravity. Requiring perturbative renormalizability means constraining such ambiguities.

Let us list some of them. A first one is combinatorial: why restricting to simplicial complexes? These are the ones for which we have a better understanding of the discrete geometry underlying our models, and in particular of the simplicity constraints that characterize them. But what other cellular complexes should be included in the theory for consistency, e.g. because corresponding to the counterterms required for taming the perturbative divergences? Others concern the underlying quantization and imposition of simplicity constraints. Being functions of the flux variables (which are non-commutative), they depend on which quantization map is chosen to quantize such variables. Different choices result in different discrete gravity actions and different simplicial path integral measures, thus different spin foam amplitudes. Also the very definition of the simplicity conditions as operator equations acting on quantum states depends on the chosen quantization map, from which follow thus different constraints on representation variables in the spin foam amplitudes. Further, the strategy by which simplicity constraints are imposed produces in general different models or versions of the same type of models (this is apparent in the Riemannian case, while in the Lorentzian one we only have experience of different versions of the EPRL model). These and other ambiguities are discussed, e.g., in [12]. Using

$SL(2,\mathbb{C})$ or $SU(2)$ data to label quantum states, which is another choice to make, also leads to potentially different models and amplitudes. Nor one should think that these ambiguities are an artefact of the GFT or spin foam formulation. They can be convincingly argued to be the counterpart of ambiguities in the definition of the canonical Hamiltonian constraint operator and, in a way, failing to fix (at least most of) them via renormalizability conditions would be the counterpart, at the background independent level, of the problem of non-renormalizability of perturbative quantum gravity on a given spacetime geometry [21]. Perturbative GFT renormalizability is thus a crucial issue, also when one looks at it from the perspective of spin foam models, simplicial path integrals or canonical loop quantum gravity.

So, where do we stand, on this important issue? For simplicial GFT models of 4d quantum gravity the answer is, unfortunately, that we are only at the very beginning. The main reasons have been already mentioned. First, we do not know enough of their symmetries to characterize the relevant theory space. Second, the amplitudes for these models are very involved and technically challenging to compute, mostly due to the fact that the imposition of simplicity constraints makes them defined not simply on Lie group manifolds but on particular sub-manifolds of these (usually not even corresponding to homogeneous spaces). Third, dominant configurations (i.e. those giving the most divergent contribution to the amplitudes) are not just flat connections or similarly simple, but correspond to richer configurations from the point of view of simplicial geometry; possibly, they correspond to (or possibly include) the whole set of Regge geometries found as saddle-point configurations in the asymptotic analysis of spin foam amplitudes and corresponding simplicial path integrals. Therefore even power counting results are hard to obtain, and the brute force analysis of divergences is not advanced enough to indicate the needed counterterms, forming the theory space. If the theory space is hard to characterize also in the simpler 3d simplicial case (corresponding to topological BF theory), at least the amplitudes are manageable enough to obtain complete power counting theorems [22], identify some counterterms [23] and nice finiteness results [24].

So computational challenges are one big obstacle. It is on this aspect that we focus in the next section, presenting some new results in the Riemannian context. These new results should be added to other ones we have on the calculation of radiative corrections and basic divergences of both Riemannian and Lorentzian simplicial spin foam models, and on explicit evaluations of their building blocks (mainly the vertex amplitudes). For a partial list, see [25][26][27][28][29][30][31][32][33] and references therein. Future progress will build on these hard-won calculations.

For a comparison, one has to look at the amount of knowledge we have accumulated on tensorial (thus colored) GFT models [7, 8, 20]. Here we know several (classes of) models which are rigorously proven to be perturbative renormalizable, comprising both abelian and non-abelian models, on homogeneous spaces, with or without gauge invariance (closure condition), in different dimensions. Divergences are associated to bubbles, i.e. cells of the complex dual to the cellular complex associated to a GFT Feynman diagram, and typically the most divergent diagrams that form the relevant theory space of renormalizable theories are melonic ones, also singled out in tensor models. However, we also know example of TGFT models which are renormalizable outside the melonic truncation [34], and these examples may be relevant also for the case of simplicial GFT models, since the structure of their divergences presents some aspects of the simplicial case.

2.2 Continuum limit and non-perturbative renormalization

GFT models of quantum gravity are bona fide QFTs, thus they possess infinite degrees of freedom, as we expect quantum gravity to do (at least thinking of it naively as a quantum theory of the gravitational field). Control over a very large number of degrees of freedom can only be achieved step by step, within some truncation scheme. With the inclusion of more and more degrees of freedom, we can expect a richer and richer set of new phenomena to be unraveled, simply because the physics of many (quantum, interacting) degrees of freedom is very different from that of few of them. In particular, we expect new phases to be revealed. Controlling the full quantum dynamics is controlling the continuum limit of GFT models, and this implies mapping out as best as we can the phase diagram of the same models. In practical terms, it means being able to evaluate the full GFT partition function, for given values of coupling constants. This is the problem of computing the full non-perturbative renormalization group flow of any given GFT model.

Given the mentioned structural connections, understanding the non-perturbative renormalization of a quantum gravity GFT model implies controlling the continuum limit of the corresponding lattice gravity path

integral and spin foam model, and the full quantum dynamics of the corresponding canonical loop quantum gravity formulation. The characterization of the continuum quantum gravity phase diagram and the identification of one phase where an effective general relativistic dynamics of spacetime can be extracted is in fact the key outstanding open issue in the field [35–38].

Where do we stand, at the non-perturbative renormalization level? Beside work on the non-perturbative RG flow of tensor models [39, 40], a lot of activity has focused on the analysis of GFT models proper [8, 20]. Two main strategies have been followed. One is based on constructive methods, mostly focusing on the resummation of the perturbative series, e.g. showing Borel summability. The other is based on functional renormalization group analysis, either (mostly) based on the Wetterich-Morris equation for the effective action, or the Polchinski equation for n-point functions. For the same reasons that limited work on perturbative GFT renormalization, little is known about the general RG flow of simplicial GFT models of 4d quantum gravity. Simplicial GFT models in 3d have been shown to be Borel summable [41, 42] and phase transitions for the GFT formulation of simplicial BF theory in any dimension has been shown to exist [43]. But no similar analysis has been carried over to the 4d gravity case, where, as mentioned, we even lack perturbative indications.

The tensorial GFT case, on the other hand, has been widely explored, mostly via functional renormalization techniques, with many results on a variety of models, again both abelian and non-abelian, with and without gauge symmetries, based on compact as well as non-compact Lie groups, in different dimensions. Concerning UV behaviour, asymptotic freedom is found in many examples and asymptotic safety is found in others [44], in various truncations, and the perturbative results have been reproduced from a non-perturbative standpoint. More results on the relevance of truncation beyond the melonic sector have been found [45], and the use of Ward identities for studying the RG flow have been explored [20]. Concerning IR behaviour (i.e. the actual continuum limit), work is more limited (and more difficult) at the analytic level, but hints have been found, in various truncations and for various models, of a non-trivial phase diagram. In particular, hints of the existence of Wilson-Fisher fixed points (often found alongside asymptotic freedom in the UV) and of broken (or condensate) phases have been obtained [34, 46], indirectly supporting parallel work on the extraction of continuum gravitational physics from such condensate phases [47–49].

Even if it is unclear, at this stage, which of these results holds also in the simplicial 4d models, with their additional quantum geometric intricacies, all this work on tensorial GFT models has certainly led to a better understanding of GFT renormalization group schemes (and flows). This will certainly turn out to be useful also for the analysis of full-blown quantum gravity models.

3 Bubble divergences and radiative corrections in GFT: some new results

In this section we report on some recent results concerning the leading order radiative corrections to N-point functions ($N \leq 6$) for the *Duflo model* and the EPRL model, whose amplitudes we have recalled above. We refer to the cited literature for more details on motivations, construction and features of these GFT (and spin foam) models. Also, we limit our presentation to a summary of results and procedures; a more detailed presentation with be left for a forthcoming publication.

3.1 A warm-up example: the 2-point function of the Ooguri GFT model

As a warm-up, we recall the general procedure to compute the degree of divergences of GFT amplitudes both in the holonomy and spin formulation of GFT models, using the simpler case of the Ooguri GFT model for 4d topological BF theory with local $SU(2)$ invariance (that is, a simplicial GFT model on four copies of $SU(2)$ and with kinetic and interaction kernels made out of delta functions only).

Analytical evaluation in group variables - For models defined on the full group manifold or a corresponding homogeneous space (as it is the case in most tensorial GFT renormalization analyses), the evaluation is often conveniently done in the group representation. It can be carried out analytically, and it proceeds as follows. We compute first the bulk or amputated amplitude $\mathcal{A}_{bulk}$ by removing all the contributions from the external of the GFT diagram $\mathcal{G}$. This amounts to extracting only the dominant leading divergence of the amplitude (subleading divergences require a more refined procedure). Then we gauge fix the the holonomies on all the

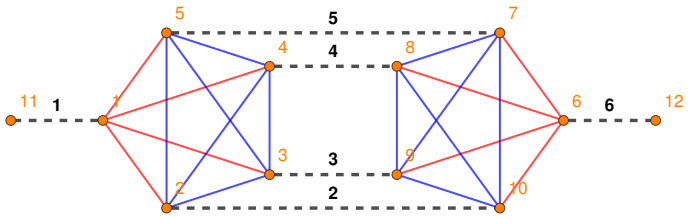

Figure 1. The picture shows the LO (melonic) radiative correction to the simplicial Ooguri model two-point function $\mathcal{W}_2$.The dashed black lines represent propagators. The solid lines encode the internal structure of each simplicial GFT vertex. A face is an alternate sequences of dashed and solid lines. Blue lines are associated to internal faces while red lines belong to the external ones. The diagram has four external and six internal faces.

edges of a maximal rooted tree of the graph $\mathcal{G}$. This reduces the evaluation to involve only a set of gauge-invariant variables. Next we drop the contribution from contractible internal faces[1] (if any). The expression so obtained is the irreducible *Master Integral* $\mathscr{I}(\mathcal{G})$ associated to the amplitude, which can then regularized introducing appropriate cut-offs on the remaining integrals (e.g. by replacing the Dirac-delta functions with heat kernels). It is important to notice that different amplitudes contributing to different correlation functions might reduce to the evaluation of the same master integral. Last we evaluate the remaining integrals. This can be done analytically, exactly or approximately for example via saddle point methods (for example using the abelian asymptotic formula for the heat kernels), to find the Master integral scaling exponent $\omega(\mathcal{G})$, i.e. its superficial degree of divergence.

Numerical evaluation in the spin basis - When the analytic evaluation in group variables is not possible, it is often more convenient to pass to the equivalent expression in terms of group representations (like the ones given above for 4d gravity models), and then proceed numerically, along similar steps as in group variables. First we compute the bulk or amputated amplitude by setting to zero all the spins labelling the external faces and using the appropriate identities for degenerate recoupling coefficients. Next we compute the Master Integral $\mathscr{I}(\mathcal{G})$, expressed in group representations, by setting to zero the spins labelling internal contractible faces. Its expression can be easily regularized by putting a uniform cutoff Λ on all unbounded summations. Last we numerically evaluate the regularized master integral as a function of the cutoff. This can be done either using the full exact formula or using its approximate asymptotic formula (for large spins) obtained by uniform rescaling of all the spins. The amplitude degree of divergence ω can then be estimated by fitting the data. More precisely it is given by the angular coefficient of the linear best fit in a Log-Log data plot.

Let us illustrate the general procedure with an example. We consider the leading order radiative (melonic) correction to the two-point function of this GFT model. The associated Feynman diagram is shown in Fig.1. The diagram has four external and six internal faces, none of which is contractible. In the holonomy formulation, the amplitude can be written as follows:

$$\mathcal{A}_{\rm Oo}(\mathcal{G}_{melon}) = \int \Big[\prod_{v\in\mathcal{G}}\prod_{e\ni v} dh_{ve}\Big] \prod_{f\in\mathcal{F}_{\rm cl}} \delta\Big[\prod_{e\in f} h_{ve}h_{v'e}^{-1}\Big] \prod_{f\in\mathcal{F}_{\rm ext}} \delta\Big[\prod_{e\in f} g_f h_{ve}h_{v'e}^{-1}\tilde{g}_f^{-1}\Big] \quad . \tag{3.1}$$

In this case, with or without gauge fixing, we can perform all the integrations exactly. Neglecting the contributions from the external faces, without a regularization we would find the divergent result:

$$\mathcal{A}_{\rm bulk}(\mathcal{G}_{melon}) = \mathscr{I}_{\rm Oo}(\mathcal{G}_{melon}) = \delta(\mathbb{I})\delta(\mathbb{I})\delta(\mathbb{I}) \quad . \tag{3.2}$$

The master integral can be regularized either via a sharp cut-off or by heat kernels:

$$\delta(g) \longrightarrow \delta_\Lambda(g) = \sum_{j=0}^{\Lambda}(2j+1)\chi^j(g) \qquad \delta(g) \longrightarrow K_\alpha(g) = \sum_{j=0}^{\infty} e^{-\alpha j(j+1)}(2j+1)\chi^j(g) \tag{3.3}$$

In both cases the amplitude's degree of divergence reads:

$$\mathscr{I}_{\rm Oo}(\mathcal{G}_{melon},\Lambda) \propto \Lambda^9 \qquad \omega(\mathcal{G}_{melon}) = 9 \quad . \tag{3.4}$$

[1] An internal face of $\mathcal{G}$ is contractible if it has at least one internal edge which is not shared with any other internal face.

The same result can be recovered by evaluating the amplitude in the spin basis. We have:

$$\mathcal{A}_{\mathrm{Oo}}(\mathcal{G}_{melon}) = \sum_{j_f | f\in\mathcal{F}_{\mathrm{cl}}} \sum_{i_{ve}} \prod_{f\in\mathcal{F}_{\mathrm{cl}}} d_{j_f} \prod_{e\in\mathcal{E}_{\mathrm{ext}}} (\mathcal{I})^{j_f i_{ve}}_{m_{ef}} \prod_{v\in\mathcal{G}} \{15 j_f\}_v \quad . \tag{3.5}$$

Since there are no contractible faces, by setting to zero all the spins labelling the external faces we immediately obtain the expression of the regularized master integral $\mathscr{I}_{Oo}$. Upon using the appropriate identify for the degenerate $15J$-symbol we find:

$$\mathcal{A}_{\mathrm{bulk}}(\mathcal{G}_{melon}, \Lambda) = \mathscr{I}_{\mathrm{Oo}}(\mathcal{G}_{melon}, \Lambda) = \sum_{j_1 j_3 j_4 j_7 j_8 j_9}^{\Lambda} d_{j_1} d_{j_3} d_{j_4} d_{j_7} d_{j_8} d_{j_9} \begin{Bmatrix} j_7 & j_3 & j_1 \\ j_9 & j_4 & j_8 \end{Bmatrix}^2 \tag{3.6}$$

$$\mathscr{I}_{\mathrm{asy}}(\mathcal{G}_{melon}, \Lambda) = \Lambda^5 \sum_{j}^{\Lambda} d_j^6 \begin{Bmatrix} j & j & j \\ j & j & j \end{Bmatrix}^2 \approx \Lambda^5 \sum_{j}^{\Lambda} j^6 j^{-3} \approx \Lambda^9 \quad . \tag{3.7}$$

Thus the degree of divergence can be obtained by evaluating the master integral's exact formula, or approximately from the above asymptotic formula, by combining the volume factor (replacing the redundant summations) and the face weights with the large-j behaviour of the Wigner $6J$-symbol, obtaining:

$$\omega_{\mathrm{full}}(\mathcal{G}_{melon}) = 8.92 \qquad \omega_{\mathrm{asy}}(\mathcal{G}_{melon}) = 9 \tag{3.8}$$

in agreement with the analytical result obtained in the group formulation.

3.2 Radiative corrections in simplicial GFT models for Quantum Gravity.

We now report on some recent results concerning the leading order radiative corrections to N-point functions ($N \leq 6$) for the Duflo model and the EPRL model.

We identify the relevant 1PI Feyman diagrams, compute the corresponding master integral formulae and use them to evaluate the master integrals' scaling (i.e. the diagrams' superficial degree of divergence) as a function of the cutoff. We also comment on the diagrams' combinatorial properties and on the structure of the corresponding counterterms. Finally we show how these results can be applied 'beyond perturbation theory'to characterize to all orders the scaling of the necklace graphs (an important subclass of diagrams appearing in the radiative correction, also identified as the relevant graphs for renormalizability in the tensorial model of [34]). We will derive first general formulae that applied to all models in the chosen class (again, simplicial models constructed from constraining those for topological BF theory) and then specialize to the models of interest by choosing the relevant form for the coefficients w, encoding the geometricity conditions characterizing them.

3.2.1 Leading order corrections to the N-point functions

The relevant 1PI GFT diagrams, appearing in the perturbative expansion of the 2-point and 4-point functions at the leading order in the GFT coupling constant λ, are shown in Tab. 1 with the notation explained in the caption. Let us make a few remarks before moving to the analysis of specific diagrams.

Selected diagrams - The diagrams showed in Fig. 1 are the only potentially divergent 1PI GFT diagrams at the leading order. All the other leading order corrections to the $3-$, $5-$ and $6-$point functions, labelled $\mathcal{G}_{311}$, $\mathcal{G}_{511}$ and $\mathcal{G}_{621}$, are manifestly convergent. The diagram $\mathcal{G}_{511}$ has no internal faces, thus no potentially divergent summation over representations. The diagrams $\mathcal{G}_{311}$ and $\mathcal{G}_{621}$ have only one internal contractible face each. Therefore their corresponding Feynman amplitudes are again finite.

$2-$*point diagrams* - The diagram $\mathcal{G}_{221}$ is melonic and therefore also tracial. It has six internal faces and four external ones and it could be expected to be the most divergent LO contribution to the 2-point function. Its dominant (or leading) divergence[2], if any, can be subtracted by mass renormalization (as done in ordinary QFT). The associated irreducible master integral will be denoted as $\mathscr{I}_{221}$. The diagram $\mathcal{G}_{222}$ has four external faces and four internal faces; one of them, the tadpole face, is contractible. The diagram $\mathcal{G}_{223}$ has four internal faces and four external ones. Although the diagram $\mathcal{G}_{222}$ and $\mathcal{G}_{223}$ are not isomorphic, their Feynman amplitudes can be reduced to the evaluation of the $4-$point function's master integral $\mathscr{I}_{421}$.

[2]The first melonic correction to the self energy might also have a subleading divergence as in the case of the Ooguri model and (Lorentzian) EPRL model. Such divergence is responsible for the wave function renormalization. This in turns requires a modification of the covariance with a second-order derivative term in order to account for the new counterterm.

Leading order corrections to the 2-point and 4-point functions.

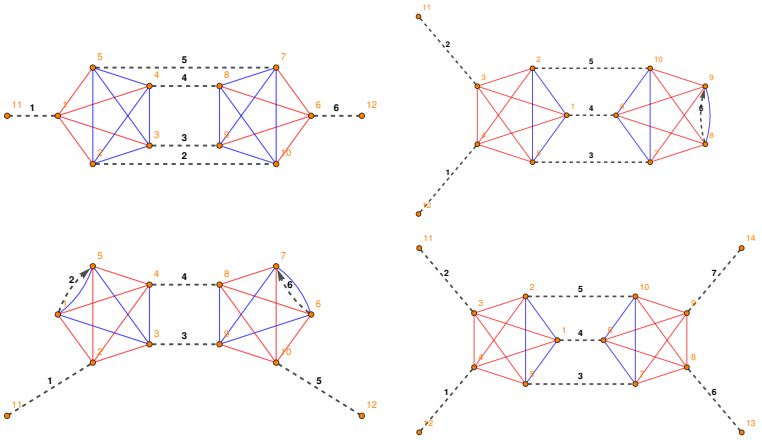

Table 1. The 1PI diagrams contributing to the LO expansion of the 2-point and 4-point functions $\mathcal{W}_2$ and $\mathcal{W}_4$. Each GFT Feynman diagram is labelled according to the number of external edges, the number of vertices and the position in the list. For example, the first graph on the left is called $\mathcal{G}_{221}$. The dashed lines represent the propagators. The solid lines denote the internal structure of each simplicial GFT vertex. Blue lines are associated to the internal faces, while red lines belong to the external ones. A face is a one-color alternating sequence of solid and dashed lines The labels for internal and external faces have not been shown.

The $4-$*point diagram* - The diagram $\mathcal{G}_{421}$ is the first melonic correction to the 4-point function. It has three internal faces (forming a bubble) and eight external ones. Its master integral $\mathscr{I}_{421}$, associated to the bubble subgraph, controls the UV scaling of the LO non-melonic 2-point diagrams and of all the necklace diagrams contributing to the N-point functions with $N = 4, 5, 6$.

To summarize: in order to determine the scaling behaviour and divergent structure of the leading corrections to the $2-$ and $4-$point functions we only need to study the independent master integrals $\mathscr{I}_{221}$ and $\mathscr{I}_{421}$, whose expression we will give and evaluate in the following.

3.2.2 The 2-point function.

To derive the expression of the master integral $\mathscr{I}_{221}$ for the leading (melonic) correction to the $2-$point function, as explained, we first write down the full regularized amplitude $\mathcal{A}(\mathcal{G}_{221}, \beta, \Lambda, \vec{J}_{\text{ext}})$ and then we set to zero all the spins associated to the external faces. Exploiting the identities (A.1, A.9, A.11) and a number of algebraic simplifications, we obtain:

$$\mathscr{I}(\mathcal{G}_{221}, l, \beta, \Lambda) = \sum_{J_f | f \in \mathcal{F}_{cl}}^{\Lambda} d_{J_1} d_{J_3} d_{J_4} d_{J_7} d_{J_8} d_{J_9} \times \mathcal{K}^{J_3 J_1 J_7}(l, \beta) \mathcal{K}^{J_4 J_7 J_8}(l, \beta) \mathcal{K}^{J_8 J_9 J_3}(l, \beta) \mathcal{K}^{J_9 J_1 J_4}(l, \beta) \begin{Bmatrix} J_7 & J_3 & J_1 \\ J_9 & J_4 & J_8 \end{Bmatrix}^2 \tag{3.9}$$

where the integer l denotes the number of simplicity constraint insertions and the propagator[3] $\mathcal{K}$ is given by the Eq. (A.12). As anticipated, in the above formula, all the model-dependent features are encoded by the single-link fusion coefficients w appearing in the expression $\mathcal{K}$, which we will refer to as the 'propagator' in the following. Thus the above result is valid for *any* simplicial GFT model for constrained BF theory.

Let us now focus on the *Duflo model*. In this case the expression (3.9) is still too complicated to be evaluated exactly, even numerically, as it stands. In order to simplify it, we use the asymptotic formula for

[3] According to the diagram's connectivity, each internal edge of the graph $\mathcal{G}_{221}$ is shared by four faces (three internal and one external). Hence, after setting to zero the external spins, the internal propagators depend only on three variables.

the $9J-$symbol (A.8). Upon introducing a new coefficient Ω_{al}

$$\Omega_{al}(j^-,j^+,\beta) \equiv \sum_{j=|j^- - j^+|}^{j^-+j^+} (2j+1)^a w^l_{Duflo}(j^-,j^+,j,\beta) \tag{3.10}$$

we can rewrite the master integral as follows:

$$\begin{aligned}\mathscr{I}_{Duflo}(\mathcal{G}_{221},l,\beta,\Lambda) = &\sum_{\text{All } j^-}^{\Lambda}\sum_{\text{All } j^+}^{\Lambda} \frac{d_{j_1^+}}{d_{j_1^-}d_{j_9^-}d_{j_3^+}d_{j_4^+}d_{j_8^+}} \begin{Bmatrix} j_7^- & j_3^- & j_1^- \\ j_9^- & j_4^- & j_8^- \end{Bmatrix}^2 \begin{Bmatrix} j_7^+ & j_3^+ & j_1^+ \\ j_9^+ & j_4^+ & j_8^+ \end{Bmatrix}^2 \\ &\Omega^2_{0l}(j_1^-,j_1^+,\beta)\Omega^2_{0l}(j_7^-,j_7^+,\beta)\Omega_{0l}(j_3^-,j_3^+,\beta)\Omega_{1l}(j_3^-,j_3^+,\beta)\Omega_{0l}(j_4^-,j_4^+,\beta) \\ &\Omega_{1l}(j_4^-,j_4^+,\beta)\Omega_{0l}(j_8^-,j_8^+,\beta)\Omega_{1l}(j_8^-,j_8^+,\beta)\Omega_{0l}(j_9^-,j_9^+,\beta)\Omega_{1l}(j_9^-,j_9^+,\beta)\end{aligned} \tag{3.11}$$

The coefficient Ω_{al} can be easily tabulated using the analytic formula for the coefficient w_{Duflo} (see eq. 1.4). The master integral (3.11) can now be numerically evaluated[4] as a function of the cutoff for different values of the parameters β and l.

In the case of the EPRL model, instead, the general formula (3.9) simplifies rather drastically[5], yielding the following result

$$\begin{aligned}\mathscr{I}_{\text{EPRL}}(\mathcal{G}_{221},l,\beta,\Lambda) = &\sum_{\text{All } j^+}^{\Lambda} d_{j_1^+}d_{j_3^+}d_{j_4^+}d_{j_7^+}d_{j_8^+}d_{j_9^+}d_{|\beta|j_1^+}d_{|\beta|j_3^+}d_{|\beta|j_4^+}d_{|\beta|j_7^+}d_{|\beta|j_8^+}d_{|\beta|j_9^+} \\ &\times \mathcal{K}^{j_3^+ j_1^+ j_7^+}(\beta)\mathcal{K}^{j_4^+ j_7^+ j_8^+}(\beta)\mathcal{K}^{j_8^+ j_9^+ j_3^+}(\beta)\mathcal{K}^{j_9^+ j_1^+ j_4^+}(\beta) \begin{Bmatrix} j_7^+ & j_3^+ & j_1^+ \\ j_9^+ & j_4^+ & j_8^+ \end{Bmatrix}^2 \begin{Bmatrix} |\beta|j_7^+ & |\beta|j_3^+ & |\beta|j_1^+ \\ |\beta|j_9^+ & |\beta|j_4^+ & |\beta|j_8^+ \end{Bmatrix}^2\end{aligned} \tag{3.12}$$

where the (degenerate) propagator $\mathcal{K}_{\text{EPRL}}$ is given by the Eq. (A.14).
A sample of the results of the numerical evaluation of the relevant master integrals[6] is in Figs. (2).
The degree of divergence $\omega(\mathcal{G}_{221})$ is given by the angular coefficient of the linear best fit of the data plotted in logarithmic scale. The mean value[7] of the scaling exponent $\bar{\omega}$ and its standard deviation for the studied cases are summarized in the table (3).

In the case of the Duflo model, some further subtlties arise in the evaluation, due to the more involved nature of the simplicity or geometricity coefficients w_{Duflo}. These subtleties require additional care in the numerical evaluation of scaling exponents, which are worth emphasizing here, since they are of more general validity in this class of spin foam amplitudes. These subtleties become even more relevant when we try to improve on the above results. Indeed, the master integral formula (3.11) relies on the use of the asymptotic formula for the $9J$-symbol (A.8). This formula might not be very accurate for relatively small spins, like the ones we can concretely explore in our numerical evaluations. Furthermore, since the (A.8) has a stronger suppression rate than other approximate formulas for the $9J$-symbol used in scaling analyses, e.g. the equilateral one $\{9j\} \approx j^{-\frac{8}{3}}$ (in which also all the js are identified, which we cannot do in the Duflo model), the full expression (3.11) is expected to provide *only* a lower bound for $\bar{\omega}$ and we also expect to be able to obtain a different scaling when relying on different asymptotic approximations. To test this expectation and also to cross-check the known EPRL results, obtained using the equilateral scaling, we repeat our analysis using in both cases a different asymptotic formula.

In order to derive another asymptotic formula for the melonic master integral $\mathscr{I}_{221}$, we localize its expression

[4] The main limitation on range of cutoff values we can test depends on the computational resources available. Here we choose $\Lambda_{\max} = 16$, $l = 1, 2$ and multiple values of β. When possible, we check for stability under extension of the range.

[5] The $9J-$symbol in the propagator (A.14) depends only on three spins, and one can use an equilateral formula, rather than the non-equilateral asymptotic formula (A.8) as for the Duflo model. Notice also that in the EPRL case there is no need to specify l, since the simplicity constraints act as a projector.

[6] They will be discussed in detail, alongside the results for other values of the various parameters, in a follow-up publication [50].

[7] To derive an estimate for ω we took the statistical average of the values obtained by fitting the data points in the cutoff ranges $\Lambda \in [\tilde{\Lambda}, \Lambda_{\max}]$ with $\tilde{\Lambda} = 7$. The lower threshold for $\tilde{\Lambda}$ corresponds to the point from where the value of ω appears to be stable within a 10% error margin (i.e. the digits to the left of the decimal point are steady).

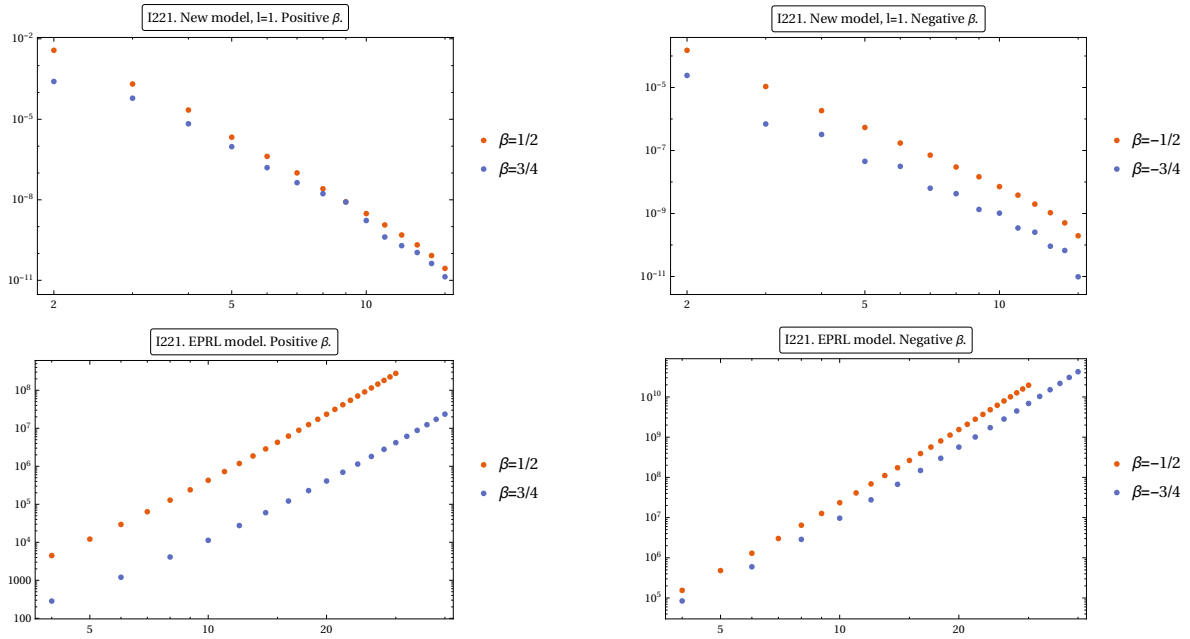

Table 2. Top: numerical evaluation of the expression $\mathscr{I}_{221}(\Lambda_{\max}) - \mathscr{I}_{221}(\Lambda)$ as a function of the cutoff $\Lambda \in [2, 16]$ in a Log-Log scale for different values of β. Here $\mathscr{I}_{221}$ is given by the master integral (3.11). Bottom: numerical evaluation of the EPRL model's master integral (3.12) as a function of the cutoff Λ and β. The cutoff ranges are $\Lambda \in [4, 30]$ for $\beta = \pm\frac{1}{2}$ and $\Lambda \in [4, 40]$ (only even values) for $\beta = \pm\frac{3}{4}$.

$\mathscr{I}_{221}$	Numerical estimates of the degree of divergence $\bar{\omega} \pm \sigma$			
β	$\frac{1}{2}$	$\frac{3}{4}$	$-\frac{1}{2}$	$-\frac{3}{4}$
Duflo model, $l = 1$.	-11.50 ± 0.85	-11.40 ± 0.51	-8.83 ± 1.06	-10.40 ± 1.94
Duflo model, $l = 2$.	-10.77 ± 0.93	-10.99 ± 0.82	-10.23 ± 0.97	-10.17 ± 0.96
Duflo model, $l = 1$. Asym.	-2.40	-1.88	-2.28	-2.20
Duflo model, $l = 2$. Asym.	-13.24	-13.4	-13.56	-13.72
EPRL model.	6.10 ± 0.04	5.95 ± 0.06	6.26 ± 0.026	6.29 ± 0.035
EPRL model. Asym	6	6	6	6

Table 3. Summary of the estimated scaling exponent $\bar{\omega}$ for leading order melonic graph $\mathcal{G}_{221}$. The EPRL values we found are in excellent agreement with other analytical results already available in the literature [26].

(3.9) around a background configuration (j^-, j^+) by setting $j_i^- = j^-$ and $j_i^+ = j^+$. For the EPRL model this also implies an homogeneous identification of all the spins j_i due to the peculiar form of the EPRL's simplicity coefficients. This procedure has been applied and tested for a number of different simplicial models, including a different version of the EPRL model [25], and it seems to be reliable [28–31, 33]. This simplification is not available for the Duflo model.

After appropriate simplifications, the general formula (3.9) becomes:

$$\mathscr{I}_{\text{asy}}(\mathcal{G}_{221}, l, \beta, \Lambda) \simeq \Lambda^{5\mu} \sum_{j^-=0}^{\Lambda} \sum_{j^+=0}^{\Lambda} d_{j^-}^6 d_{j^+}^6 \left[\mathcal{K}^{j^- j^+}(l, \beta)\right]^4 \begin{Bmatrix} j^- & j^- & j^- \\ j^- & j^- & j^- \end{Bmatrix}^2 \begin{Bmatrix} j^- & j^+ & j^+ \\ j^+ & j^+ & j^+ \end{Bmatrix}^2 \tag{3.13}$$

where $\mu = 1, 2$, for the EPRL and Duflo models. The reduced propagator $\mathcal{K}^{j^- j^+}$ is given by the Eq. (A.13). To determine the amplitude's degree of divergence we combine the scaling of the various factors. The scaling of the equilateral $6J$-symbol is given by the Regge formula $\{6j\} \approx j^{-\frac{3}{2}}$. According to our analysis, in the

large-j regime the propagator (A.13) can be very well approximated by the following expressions:

$$\mathcal{K}^{j^-,j^+}_{Duflo}(l,\beta) \simeq \frac{\delta_{j^- |\beta| j^+}}{(2j^+ + 1)^{\alpha}} \qquad \mathcal{K}^{j^- j^+}_{\text{EPRL}}(\beta) \simeq \frac{\delta_{j^- |\beta| j^+}}{(2j^+ + 1)^{\frac{3}{2}}} \qquad \alpha = \alpha(l,\beta) \tag{3.14}$$

The EPRL formula can be analytically derived, as shown in Appendix A (see A.15, A.16). The corresponding formula for the Duflo model follows from a direct numerical evaluation of the propagator. It is worth noticing that also the Duflo propagator, containing the much more involved Duflo geometricity coefficients (1.4), peak on the same configurations of $Spin(4)$ representations (j^+, j^-). This is due to the asymptotic behaviour of such coeffcients, which contains also (but not only) the configurations corresponding to the EPRL configurations among the dominant ones [51][8].
The computed values of the scaling exponent α can be found in the table (4).

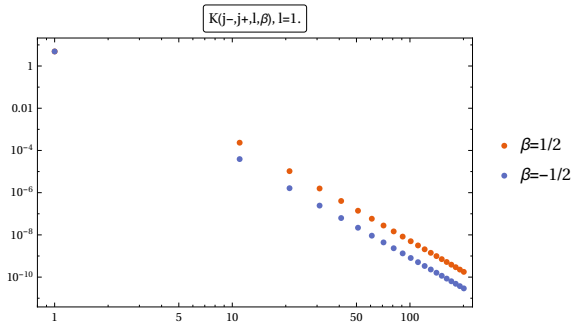

Numerical values of α				
l	$\frac{1}{2}$	$\frac{3}{4}$	$-\frac{1}{2}$	$-\frac{3}{4}$
$l=1$	4.85	4.72	4.82	4.80
$l=2$	7.56	7.60	7.64	7.68

Table 4. Left panel: numerical evaluation of the propagator $\mathcal{K}_{Duflo}$ with $l = 1$ and $j^- = |\beta| j^+$ in a logarithmic scale. Right panel: computed estimates of the propagator's scaling exponent α for various values of β and l.

The values of ω, obtained by substituting the identities (3.14) into the master integral formula (3.13), are listed in table (3).

To summarize: the leading order (melonic) correction to the self-energy (3.9) appears to be convergent for the Duflo model and divergent for the EPRL one. The degree of divergence we computed for the EPRL model is in excellent agreement with known analytical results in the literature [25, 26]. Concerning the Duflo model for the case $l = 1$ the data clearly indicates that the use of the non-equilateral formula (A.8) in (3.11), as appropriate for this model, strongly suppresses the amplitude scaling leading to a more convergent result. This might also be true for the case $l = 2$ although we cannot state it with full confidence at the moment based on the small cutoff range we tested (recall that $\Lambda_{\max} = 16$ in the full formula and $\Lambda_{\max} = 100$ in the asymptotic formula). The limited range of Λ values we explored might also explain why the difference between the values of ω for $l = 1, 2$ computed from (3.11) (first and second row of Tab. 3) is smaller than the difference between the corresponding values obtained from the asymptotic formula (third and fourth row of Tab. 3).

3.2.3 The 4-point function.

We now focus on the leading (melonic) correction to the 4-point function. The corresponding GFT Feynman diagram $\mathcal{G}_{421}$ is depicted in table (1). In order to derive the master's integral expression we follow the same strategy used in the previous section. After setting to zero the spins labelling the external faces and performing the appropriate simplification we find:

$$\mathscr{I}(\mathcal{G}_{421}, l, \beta, \Lambda) = \sum_{j_1^-, j_1^+}^{\Lambda} \sum_{j_{31} j_{41} j_{51}} \frac{d_{j_{31}} d_{j_{41}} d_{j_{51}}}{d_{j_1^-} d_{j_1^+}} w^l(j_1^-, j_1^+, j_{31}, \beta) w^l(j_1^-, j_1^+, j_{41}, \beta) w^l(j_1^-, j_1^+, j_{51}, \beta) \tag{3.15}$$

Once more, the above formula is completely general and valid for any simplicial GFT (spin foam) model for constrained BF theory.

[8] From this fact, one could conclude that the Duflo model also includes the same semi-classical configurations of the EPRL model, in addition to other ones, whose discrete geometric meaning should be explored.

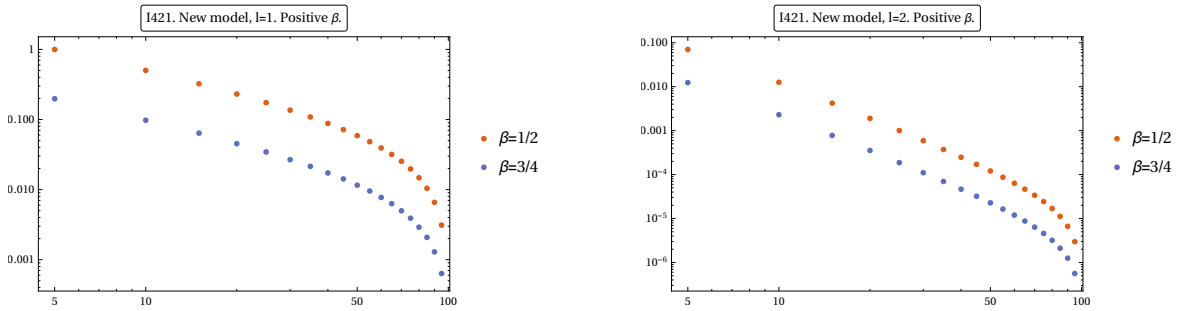

Table 5. Numerical evaluation of the expression $\mathscr{I}_{221}(\Lambda_{\max}) - \mathscr{I}_{221}(\Lambda)$ as a function of the cutoff $\Lambda \in [5, 100]$ in a Log-Log scale for different values of l and β. Here $\mathscr{I}_{421}$ is given by the Master integral formula (3.16).

For the EPRL and Duflo models it specializes to:

$$\mathscr{I}_{Duflo}(\mathcal{G}_{421}, l, \beta, \Lambda) = \sum_{j_1^-, j_1^+}^{\Lambda} \frac{1}{d_{j_1^-} d_{j_1^+}} \left[\Omega_{1l}(j_1^-, j_1^+, \beta)\right]^3 \tag{3.16}$$

$$\mathscr{I}_{\text{EPRL}}(\mathcal{G}_{421}, \beta, \Lambda) = \sum_{j_1^-=0}^{\Lambda} \frac{(2(1-\beta)j_1^+ + 1)^3}{(2j_1^+ + 1)(2|\beta|j_1^+ + 1)} \tag{3.17}$$

where in the first expressions we used the same notations of (3.11).
The degree of divergence of the master integral (3.16) can be computed again by fitting the data. The resulting values of ω are reported in Tab. (6).

$\mathscr{I}_{421}$	Numerical estimates of the degree of divergence $\bar{\omega} \pm \sigma$	
β	$\pm\frac{1}{2}$	$\pm\frac{3}{4}$
Duflo model, $l = 1$.	-2.36 ± 0.24	-2.35 ± 0.24
Duflo model, $l = 2$.	-3.67 ± 0.20	-3.67 ± 0.20

Table 6. Numerical values of the divergence's degree for the 4-point amplitude $\mathscr{I}_{Duflo}$.

The scaling of the EPRL 4-point amplitude can be directly read off from the corresponding formula (3.17).

$$\omega(\mathcal{G}_{421}) = 2 \qquad \beta \neq 0, \pm 1 \tag{3.18}$$

To summarize: the leading order radiative correction to the 4-point function converges for the Duflo model while it diverges quadratically in the EPRL model.
More than the divergence degree in itself, it is important to notice that, since the $\mathcal{G}_{421}$ is melonic (and thus tracial), the corresponding counterterm that is required to absorb the divergence, when present, is proportional to a tensor invariant quartic interaction term (more precisely to the bubble B_{41} vertex in Fig. 2). Such counterterm is incompatible with a pure simplicial theory space (e.g. a strictly simplicial EPRL model would be non-renormalizable), and this signals the need to extend the theory space of geometric GFT models beyond the simplicial ansatz to include tensorial bubble interactions.

3.2.4 Next-to-leading order corrections to the N-point functions.

We now show how to generalize the master integral formulas for the melonic 2-point function $\mathcal{G}_{221}$ to an important class of higher order GFT Feynman diagrams.
The master integral expressions (3.9, 3.13) rely on the property that each internal link of the diagram is shared exactly by one external face and three internal ones. Hence, after setting to zero the spins labelling the external

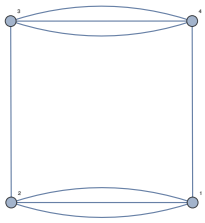

Figure 2. The quartic tensorial bubble interaction B_{41}.

faces we are left with: i) a pair of $6J$-symbols for each vertex (coming from a pair of degenerate $15J$-symbols); ii) propagator of the form (A.12) for each internal edge. A pair of face weights $d_{j_i^-} d_{j_i^+}$ for each internal face. The above combinatorial property is true for any tadpole-free GFT diagram with one and only one external link for each simplicial vertex (here denoted as $\mathcal{G}_{N_v N_v n}$). Some examples of these diagrams are shown in Fig. (3). Therefore the expression (3.13) can be generalized as follows:

$$\mathscr{I}(\mathcal{G}_{N_v N_v n}, l, \beta, \Lambda) = \sum_{J_f \in \mathcal{F}_{\rm cl}}^{\Lambda} \prod_{f \in \mathcal{F}_{\rm cl}} d_{J_f} \prod_{e \in \mathcal{E}_{\rm int}} \mathcal{K}^{J_{f_i} J_{f_j} J_{f_k}}(l, \beta) \prod_{v \in \mathcal{V}} \{6J_{vf}\} \tag{3.19}$$

$$\mathscr{I}_{\rm asy}(\mathcal{G}_{N_v N_v n}, l, \beta, \Lambda) = \Lambda^{(N_f-1)\mu} \sum_{j^-, j^+}^{\Lambda} d_{j^-}^{N_f} d_{j^+}^{N_f} \left[\mathcal{K}^{j^- j^+}(l, \beta)\right]^{N_e} \begin{Bmatrix} j^- & j^- & j^- \\ j^- & j^- & j^- \end{Bmatrix}^{N_v} \begin{Bmatrix} j^- & j^+ & j^+ \\ j^+ & j^+ & j^+ \end{Bmatrix}^{N_v} \tag{3.20}$$

with $\mu = 1, 2$ respectively for the EPRL and the Duflo model.
Upon using the identities (3.14), the asymptotic master integral (3.20) takes the following form:

$$\mathscr{I}_{\rm asy}(\mathcal{G}_{N_v N_v n}, l, \beta, \Lambda) \simeq \Lambda^{(N_f-1)\mu} \sum_{j^+}^{\Lambda} \left(j^+\right)^{2N_f - \alpha N_e - 3N_v} = \Lambda^{(\mu+2)N_f - 3N_v - \alpha N_e - \mu + 1} \tag{3.21}$$

$$\omega(\mathcal{G}_{N_v N_v n}) = (\mu+2)N_f - 3N_v - \alpha N_e - \mu + 1 \tag{3.22}$$

For the Duflo model the value of α must be computed on case by case basis (see Tab. 4), while for the EPRL model we have $\alpha = \frac{3}{2}$.
The degree of divergence ω can also be written in terms of the number of vertices N_v

$$\omega(\mathcal{G}_{N_v N_v n}) = (\mu+2)N_f - (2\alpha+3)N_v - \mu + 1 \qquad N_e = \frac{5N_v - N_{\rm ext}}{2} = 2N_v \tag{3.23}$$

For the diagrams in Fig. (3) the above formula give us the following results, reported in the table (7): the Duflo model amplitudes for all four diagrams are finite; for the EPRL model[9] the first and last diagrams might be logarithmically divergent and therefore require a deeper analysis [50]. The diagram $\mathcal{G}_{442}$ converges, while the melonic diagram $\mathcal{G}_{441}$ diverges as a cubic power of the cutoff. The corresponding counterterm is proportional to the quartic bubble vertex B_{41}, suggesting again the need for a suitable extension of the theory space to incorporate the relevant tensorial interactions.

3.2.5 Beyond perturbation theory: the necklace diagrams

In the previous two subsections we discussed the all the leading order and a subclass of next-to-leading order radiative corrections to the N-point functions with $N \leq 6$. Now we show how to use some of the results we found to estimate the scaling of the so-called necklace diagrams to all orders in perturbation theory.
A (connected) GFT Feynman diagram belongs to the necklace class if (and only if) it consists of an open chain of vertices where each vertex (except the first and last ones) is connected only to its two closest neighbours. Here we restrict to the set of k-necklace diagrams with $4 \leq k \leq 6$ where k denotes the number of external links, since all other higher order diagrams are either 1-particle reducible or manifestly convergent. Three examples of necklace diagrams are shown in Tab. (8). The necklace diagrams share the following remarkable property:

[9] We point out again that we are studying both models under specific choices fixing the various ambiguities that enter the construction of the spin foam amplitudes. These ambiguities affect, in general, the scaling results.

NLO corrections to the 3-point and 4-point functions.

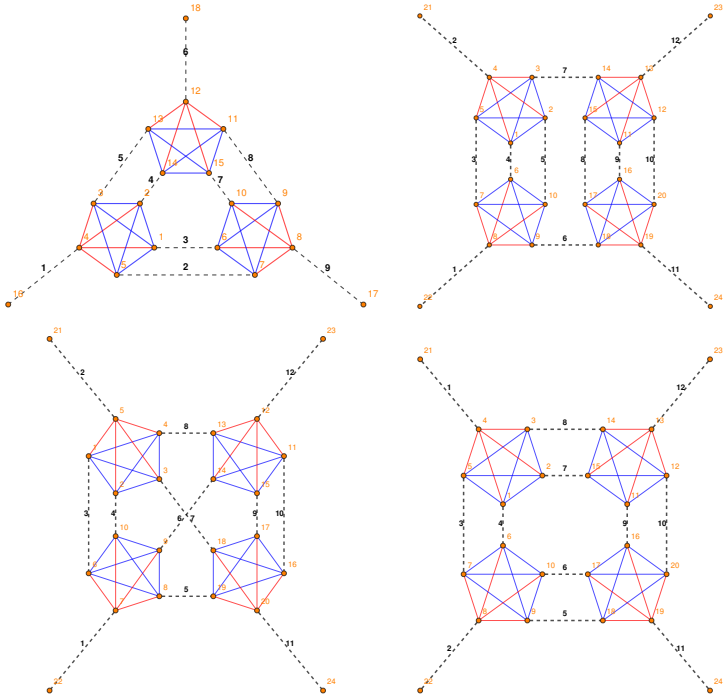

Figure 3. Example of GFT diagrams of the type $\mathcal{G}_{N_v N_v n}$ contributing to the 3− and 4−point functions at the NLO.

Degree of divergence. NLO graphs.

$\mathcal{G}$	$\mathcal{G}_{331}$	$\mathcal{G}_{441}$	$\mathcal{G}_{442}$	$\mathcal{G}_{443}$
Duflo model, $l=1$, $\beta=\frac{1}{2}$.	-15.1	-15.8	-31.8	-19.8
EPRL model	0	3	-9	0

Table 7. Degree of divergence for the diagrams in fig. 3 computed from the power counting formula (3.23).

the set of internal faces of a k-necklace diagram can always be decomposed into the direct sum of two subsets

$$\mathcal{F}(\mathcal{G}_{k-\text{necklace}}) = \bar{\mathcal{F}} \oplus \tilde{F} \qquad \bar{\mathcal{F}} = \oplus_{i=1}^{N_b} \mathcal{F}_{\mathcal{B}_{421}} \qquad \tilde{\mathcal{F}} = \{f_j \mid f_j \text{ contractible } \forall j\} \tag{3.24}$$

where the (three) faces in each set $\mathcal{F}_{\mathcal{B}_{421}}$ form the bubble subgraph $\mathcal{B}_{421}$ of the melonic 4-point diagram $\mathcal{G}_{421}$ while the faces in $\tilde{\mathcal{F}}$ are contractible. The integer N_b, namely the number of disjoint bubbles $\mathcal{B}_{421}$ depends on the connectivity of the necklace diagram itself (i.e. on its number of vertices and external links). Thus after setting to zero the spins labelling the external and the contractible internal faces, the amplitude of k-necklace diagram factorizes into N identical copies of the master integral $\mathscr{I}_{421}$ given in (3.15). More in detail, we have:

$$\mathcal{A}(\mathcal{G}_{k-\text{necklace}}, l, \beta, \Lambda) = [\mathscr{I}(\mathcal{G}_{421}, l, \beta, \Lambda)]^{\frac{N_v - \text{mod}(k,2)}{\lfloor k,2 \rfloor}} \tag{3.25}$$

To summarize: the master integral $\mathscr{I}_{421}$ encodes the scaling of the necklace diagrams to all orders in perturbation theory. For the EPRL model a consistent (recursive) subtraction of all divergences associated to k-necklace graph requires an extension of the theory space to include the appropriate tensor invariant interactions of order four and six. A more detailed analysis of the combinatorial structure of the require counterterms is left for future work [50].

GFT necklace graphs

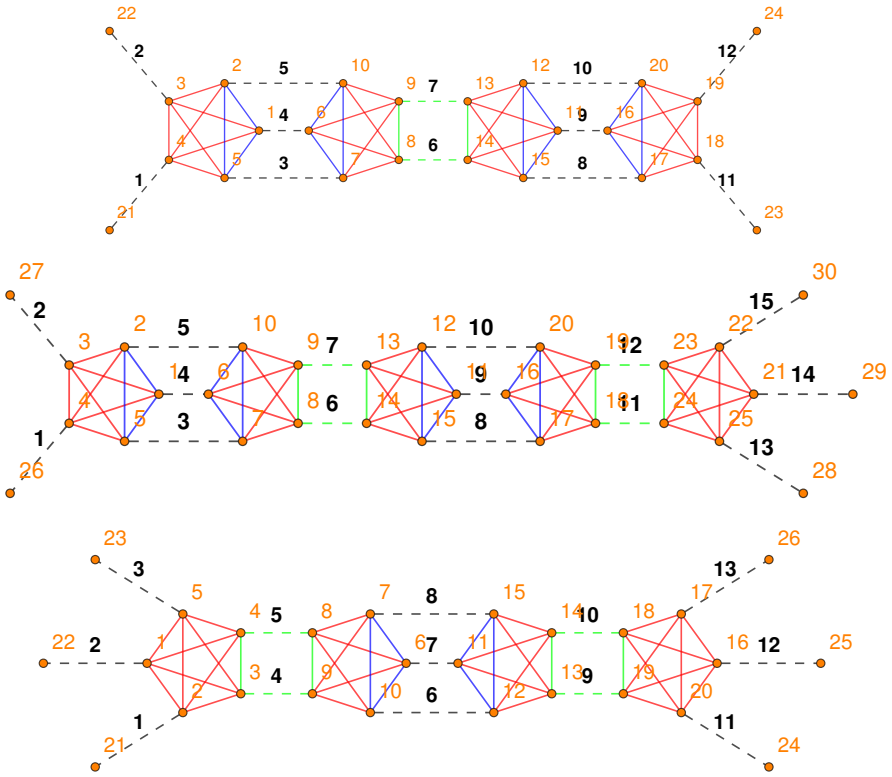

Table 8. Examples of necklace diagrams contributing to the 4−, 5− and 6−point functions

4 The road ahead: some suggestions

We close with a set of suggestions for research directions to be pursued, toward a complete understanding the renormalization group flow of simplicial GFT models for 4d quantum gravity.

4.1 Scaling and more scaling, and the discrete geometry of divergent configurations

The first suggestion is stating the obvious: compute, compute, compute. We need to (pardon us the word pun) scale up the effort in investigating the scaling of simplicial GFT amplitudes, at the same time trying to import insights from tensorial GFT amplitudes. We need to know much more about the divergent configurations and their dependence on the combinatorics of the underlying cellular complex. Lacking better tools, hard brute-force computations of spin foam amplitudes are the inevitable duty, and these in turn can only build on a better control of the relevant buliding block the vertex amplitude or, in GFT language, the vertex kernel (which plays an important role also in non-perturbative calculations). Brute force alone will not lead us far, however. On the one hand, we need to develop a more refined analytic understanding of these kernels and resulting amplitudes, and to identify simplified expressions that capture the relevant scaling properties, and their behaviour under coarse-graining. On the other hand, where analytical methods do not reach, we need numerical ones to take over; numerical tools for the evaluation of GFT amplitudes are thus badly needed. Packages like have been developed for local QFT Feynmanology would be of course most welcome. On the analytic side, another important objective should be to characterize in detail the (simplicial) geometric meaning of the dominant, most divergent configurations. This is needed to understand the nature of the needed counterterms, but it may also provide insights on the physical features of such GFT models, even beyond their discrete formulation.

The goal here is not to so much to be able to compute GFT Feynman diagrams to arbitrary order (e.g. in vertex or loop expansions). Even in standard QFT, for the physical questions for which the perturbative expansion is the correct approximation scheme, we need to compute (very) many diagrams, but there is often

no need nor possibility to go beyond some (usually low) order of approximation and beyond a certain (usually small) number of physical degrees of freedom in the chosen boundary states (of course, the two restrictions go together, since for highly populated boundary states, even the simplest diagrams are of high order). A clear physical picture behind this approximation scheme is as important as computational power. Moreover, coming to the specific quantum gravity case, we would argue that the perturbative GFT expansion, and the description of the dynamics in terms of elementary processes involving few of the fundamental quanta, ie. the usual spin foam language, is not the most convenient approximation to capture the effective continuum physics of quantum gravity, e.g. concerning early cosmology or quantum black holes.

Nor the goal of such analysis of perturbative GFT divergences is establishing that one specific GFT model is finite. Not only renormalizability is a more subtle and possibly interesting feature that finiteness, but one can imagine playing with the ambiguities entering the construction of any given model to modify its scaling behaviour and turning it into a finite one. This could be a way to fix or constrain such ambiguities, of course, but it also shows that finiteness per se probably should not be a goal, and that physical conditions fixing the same ambiguities are needed. The main goal of actual computations of GFT amplitudes should then be to provide solid indications on the general power counting of divergences, on the way to a renormalizability proof, and, even more, to indicate the relevant counterterms to be added to the model, and thus the relevant theory space of the starting GFT model. More generally, the goal of such perturbative calculations should be to provide information and tools to be employed to go beyond the perturbative setting and dwell into non-perturbative GFT renormalization. It is only the latter that can provide us with the insights and the results we need to truly explore the formal solidity and effective continuum physics of GFT models of quantum gravity.

4.2 GFT theory space, colors and relation between simplicial and tensorial models

We have emphasized several times already the importance of defining the relevant theory space of simplicial GFT models, in order to set up a proper renormalization scheme (perturbative and non-perturbative). Much more work should be devoted to this issue, in particular understanding more about the symmetries of such quantum gravity models. One question is whether the yet to be identified theory space of simplicial GFT models relates to the one of tensorial GFTs. We speculate that they do and, in fact, some hints that the two may largely coincide are known. First, taking seriously the tensorial nature of GFT fields implies coloring (thus distinguishing and ordering) their arguments and, as a consequence, their Feynman diagrams. As we noted, this coloring allows a precise control over the topology of the cellular complexes dual to these Feynman diagrams [4] and, in turn, this greater control allowed for many results that are central in renormalization analyses of tensorial GFTs (e.g. large-N expansions) [7, 8]. A precise control over the topology of the Feynman diagrams, i.e. the cellular complexes on which spin foam amplitudes are based, is needed also in simplicial GFTs, if one aims at identifying the nature of divergences, leading to precise power counting results. It is also needed for identifying key symmetries, as we know already in the case of topological BF models [52], where the complete power counting also relied on the full topological information on the underlying cellular complex [22]. Thus we have a strong argument for relying on colors also in simplicial GFT models of 4d quantum gravity; the form of the corresponding spin foam amplitudes would remain unchanged, but they would now be defined on full 4d cellular complexes, rather than just their 2-skeleton. Assuming we work on colored simplicial GFT models, we then have two preliminary results that suggest a close relation with tensorial models. One is that using colors one can identify similar symmetries in the simplicial case than one finds in the tensorial one [53]. The other is that integrating out all fields except one in a colored simplicial GFT model (in any dimension, with trivial kinetic term) produces an equivalent tensorial GFT model for the remaining field (with the same coupling constant for all interactions) [54]. A third general fact pointing in the same direction is that divergences in simplicial GFT models for topological BF theory, which is the starting point of the construction of simplicial 4d gravity models, are associated to bubbles in the cellular complex, which are in fact the cells associated to allowed interactions in tensorial GFTs with the same base group manifold. These results, in our opinion, suggest that there could be a single theory space containing both (colored) simplicial models and tensorial ones, with interaction kernels in the tensorial directions yet to be identified.

4.3 GFT models with local directions

The third suggestion for further research is to devote attention to the renormalization of GFT models which combine the combinatorially non-local pairing structure on geometric variables, in GFT interactions, with the presence of local directions. This includes both simplicial GFT models and tensorial ones, with the distinction referring to the pairing of geometric variables.

There are two main examples of such 'mixed'models. One is the tensorial models used to describe SYK-like many-body systems [55], whose renormalization has been in fact studied in several cases. Here the non-local, tensorial indices are usually reduced to finite sets (we have thus simple tensor models, rather than full GFTs) and the single local direction is a time variable. The standard SYK models are indeed quantum mechanical models in 0+1 dimensions, with generalizations to higher dimensions (thus, with more local directions) having been proposed. The other class of mixed models is the extension of (simplicial) GFT quantum gravity models to include scalar fields coupled to gravitational degrees of freedom [56]. These extended models have been studied in particular in the context of GFT condensate cosmology [47–49, 57, 58], with the additional scalar fields playing (also) the role of clock and rods that allow to define relational, diffeo-invariant observables in terms of which an effective cosmological dynamics can be extracted from the GFT hydrodynamics.

The potential physical interest of these models, and of their renormalization analysis, is thus obvious. They present several interesting issues. The presence of both local and non-local directions may modify sensibly the renormalization flow and the structure of divergences, thus leading to different dominant diagrams and effective dynamics in both UV and IR sectors. One can also envisage setting up an altogether different renormalization group scheme, adopting a notion of scale tied to the scalar (local) directions, rather than the group manifold (or involving both), potentially producing very different results. Such focus on the flow parametrised by variables with a (tentative) physical interpretation as relational time/space variables may also allow a more direct physical interpretation of the renormalization flow itself, e.g. in a cosmological context (even though similar cautionary remarks as for the usual renormalization scheme would apply here).

4.4 Relation with lattice spin foam renormalization

We have emphasized how renormalizing a GFT model is tantamount to renormalizing (and studying the continuum limit of) the corresponding discrete gravity path integral and spin foam amplitudes, from a different standpoint. But the GFT formalism is only one way to provide a complete definition of spin foam models, the other being to view them as a peculiar (because background independent) lattice theory and setting up some appropriate refinement procedure. Therefore, it would be very important to compare results obtained in the context of GFT renormalization, especially for simplicial quantum gravity models, with the results and techniques developed for renormalizing spin foam amplitudes from a lattice gauge theory perspective [37, 38, 59–61].

In this lattice-focused approach to spin foam renormalization, a cut-off is also imposed on representation variables, but the notion of 'scale'is rather given by the combinatorial complexity of the underlying lattice, and the renormalization group flow is driven by refinement/coarse-graining steps ordered by such complexity. Refinement/coarse-graining steps affect both bulk lattices and boundary graphs, and the flow of quantum amplitudes is constrained by the requirement of their consistency under restriction to coarser boundary states.

Despite their differences, the two renormalization schemes share several, since also GFT subtraction moves amount to lattice coarse-graining steps, and corresponding maps between associated amplitudes are also built-in in the (perturbative) QFT renormalization steps used in the GFT context. Still, a detailed work of translation between the two frameworks would be very useful. This work may require, on the GFT side, a combination of functional renormalization group techniques, since we are interested in the continuum limit of spin foam models, and perturbative expansions, given that spin foam models arise in such expansion. This comparison would be beneficial for both approaches; in particular, it would emphasize the role of combinatorial complexity of boundary states in the GFT renormalization flow. This work should be carried out for all models that have been studied in both settings (also in the lattice renormalization approach work has been confined mostly to highly simplified models), aiming of course at unraveling the continuum phase diagram of 4d quantum gravity from two perspectives at once.

4.5 GFT renormalization via tensor networks

One powerful set of techniques coming from the theory of quantum many-body systems, that have been already applied in the context of lattice-based renormalization of spin foam models, uses the language of tensor networks [62, 63]. This language is useful both for numerical studies and for emphasizing the role of entanglement in the renormalization group flow [64, 65]; in particular, it allows to unravel topological quantum phases of many-body systems.

In the case of GFT models, the interest in importing techniques from tensor networks goes beyond these general facts, and stems also from the fact that GFT states themselves can be seen as generalised tensor networks [66], and by the related fact that entanglement is responsible for the basic connectivity between GFT quanta that gives rise to extended discrete structures labeled by quantum geometric data. The many facets of the GFT formalism, moreover, would allow for a manifold application of tensor network techniques. On the one hand the basic GFT field is a tensor and its quantum states are tensor networks, as mentioned; on the other hand, it remains a QFT, calling for continuum tensor network techniques as employed, say, in standard scalar quantum field theory [67]. At the same time, its Feynman amplitudes are lattice gauge theories, to which a different set of tensor network techniques can be applied [68] (as developed in the context of spin foam lattice renormalization). And they remain quantum many-body systems, peculiar for their background independent nature, but still conventional enough to allow the deployment of tensor network methods taken from their natural context.

A Useful identities.

A.1 $9J$-symbol.

In this note we only need the identities regarding to types of degenerate $9J$-symbols.

Type A. One degenerate triad. This type of $9J$-symbol occurs in the evaluation of the bulk amplitudes.

$$\begin{Bmatrix} 0 & j_2 & j_3 \\ 0 & j_5 & j_6 \\ 0 & j_8 & j_9 \end{Bmatrix} = \delta_{j_2 j_3} \frac{(-1)^{j_3+j_6+j_8}}{\sqrt{(2j_3+1)}} \begin{Bmatrix} j_9 & j_6 & j_3 \\ j_5 & j_8 & 0 \end{Bmatrix} = \delta_{j_2 j_3}\delta_{j_5 j_6}\delta_{j_8 j_9} \frac{1}{\sqrt{(2j_3+1)(2j_6+1)(2j_9+1)}} \tag{A.1}$$

Type B. One row is the sum or the difference of the other two. The type B $9J$-symbols occur in the full and asymptotic formulas of the EPRL 2-point master integral $\mathscr{I}_{221}$. In detail, we have:

$$\begin{Bmatrix} bj_1^+ & bj_2^+ & bj_3^+ \\ j_1^+ & j_2^+ & j_3^+ \\ aj_1^+ & aj_2^+ & aj_3^+ \end{Bmatrix} \underset{\beta<0}{\approx} \left[\frac{4a}{b\pi}\right]^{\frac{1}{4}} \Delta(j_1^+, j_2^+, j_3^+) \left[\frac{1+a(j_1^+ + j_2^+ + j_3^+)}{(1+2aj_1^+)(1+2aj_2^+)(1+2aj_3^+)(1+j_1^+ + j_2^+ + j_3^+)}\right]^{\frac{1}{2}} \tag{A.2}$$

$$\begin{Bmatrix} bj_1^+ & bj_2^+ & bj_3^+ \\ \delta j_1^+ & \delta j_2^+ & \delta j_3^+ \\ j_1^+ & j_2^+ & j_3^+ \end{Bmatrix} \underset{\beta\geq 0}{\approx} \left[\frac{4}{b\pi\delta}\right]^{\frac{1}{4}} \Delta(j_1^+, j_2^+, j_3^+) \left[\frac{1+j_1^+ + j_2^+ + j_3^+}{(1+2j_1^+)(1+2j_2^+)(1+2j_3^+)(1+\delta(j_1^+ + j_2^+ + j_3^+))}\right]^{\frac{1}{2}} \tag{A.3}$$

where, for convenience of notation, we have used the following conventions:

$$b = |\beta| \qquad a = 1+b = 1+|\beta| \qquad \delta = 1-b = 1-|\beta| \tag{A.4}$$

$$\Delta(j_1^+, j_2^+, j_3^+) = \left[\frac{j_1^+ j_2^+ j_3^+ (1+b(j_1^+ + j_2^+ + j_3^+))^{-2}}{(j_1^+ + j_2^+ - j_3^+)(j_1^+ - j_3^+ + j_3^+)(-j_1^+ + j_2^+ + j_3^+)(j_1^+ + j_2^+ + j_3^+)}\right]^{\frac{1}{4}} \tag{A.5}$$

The EPRL $9J$-symbol (type B) can be easly tabulated compared to the full $9J$-symbol. Upon identifying all three triads we obtain the following asymptotic formulas:

$$\begin{Bmatrix} bj^+ & bj^+ & bj^+ \\ j^+ & j^+ & j^+ \\ aj^+ & aj^+ & aj^+ \end{Bmatrix} \underset{\beta<0}{\approx} \left[\frac{4a}{3\pi b}\right]^{\frac{1}{4}} \left[\frac{1+3aj^+}{\sqrt{j^+}(1+3j^+)(1+3bj^+)(1+2aj^+)^3}\right]^{\frac{1}{2}} \underset{j\to+\infty}{\approx} j^{-\frac{9}{4}} \tag{A.6}$$

$$\begin{Bmatrix} bj^+ & bj^+ & bj^+ \\ \delta j^+ & \delta j^+ & \delta j^+ \\ j^+ & j^+ & j^+ \end{Bmatrix} \underset{\beta\geq 0}{\approx} \left[\frac{4}{3\pi\delta b}\right]^{\frac{1}{4}} \left[\frac{1+3j^+}{\sqrt{j^+}(1+3bj^+)(1+3\delta j^+)(1+2j^+)^3}\right]^{\frac{1}{2}} \underset{j\to+\infty}{\approx} j^{-\frac{9}{4}} \tag{A.7}$$

Last we provide a general asymptotic formula for $9J$-symbol which, according to [69], is valid when all the spins are large but distinct.

$$\left|\begin{Bmatrix} j_1 & j_2 & j_3 \\ j_4 & j_5 & j_6 \\ j_7 & j_8 & j_9 \end{Bmatrix}\right| \underset{j_i \gg 1}{\approx} \frac{L}{\sqrt{(2j_1+1)(2j_2+1)(2j_4+1)(2j_6+1)(2j_8+1)(2j_9+1)}} \qquad L>1 \tag{A.8}$$

This formula should be used cautiously since it might not be quite accurate for small spins (e.g. $j \approx 10$). Moreover, it seems to enhance the $9J$-symbol's fall-off rate compared to the above listed formulas.

A.2 $15J$-symbol.

The $15J$-symbol (of the first type) can be written either as a single sum of five $6J$-symbols [69]. We call *tetrad* the set of spins emanating from a given node of the $15J$-symbol graph Γ_5. The $15J$-symbol with one vanishing tetrad obeys the following formula:

$$\begin{Bmatrix} i_1 & 0 & i_3 & j_4 & i_5 \\ 0 & j_7 & j_8 & j_9 & 0 \\ j_1 & i_2 & j_3 & i_4 & 0 \end{Bmatrix} = (-1)^{j_1+j_7+j_8+j_9} \frac{\delta_{i_2 i_5}\delta_{i_2 j_1}\delta_{i_5 j_1}\delta_{i_3 j_7}\delta_{i_4 j_9}}{(2j_1+1)\sqrt{(2j_7+1)(2j_9+1)}} \begin{Bmatrix} j_7 & j_3 & j_1 \\ j_9 & j_4 & j_8 \end{Bmatrix} \tag{A.9}$$

All other formulas can be derived in the same way directly from the definition.

A.3 Fusion coefficients and propagators.

The fusion coefficients are defined as the matrix elements (in the quantum number basis) of a map between the spaces of 4-valent Spin(4) and SU(2) intertwiners.

$$f_I^{i,l}(J_p, j_p, k, \beta) = \sum_{M_p m_p} (\mathcal{I})^{J_1 J_2 J_3 J_4 I}_{M_1 M_2 M_3 M_4} \left[\prod_{p=1}^{4} C^{j_p^- j_p^- j_p}_{m_p^- m_p^- m_p}(k) w^l(J_p, j_p, \beta)\right] (\mathcal{I})^{j_1 j_2 j_3 j_4 i}_{m_1 m_2 m_3 m_4} \tag{A.10}$$

Uppercase letters denote Spin(4) representations and intertwiners while lowercase letters label SU(2) data. Upon using the appropriate recoupling identities they can be rewritten as shown below.

$$f_I^{i,p}(J_l, j_l, \mathbb{I}, \beta) = (-1)^S \left[\prod_{l=1}^{4} w^p(J_l, j_l, \beta)\right] \begin{Bmatrix} j_1^- & i^- & j_2^- \\ j_1^+ & i^+ & j_2^+ \\ j_1 & i & j_2 \end{Bmatrix} \begin{Bmatrix} j_3^- & i^- & j_4^- \\ j_3^+ & i^+ & j_4^+ \\ j_3 & i & j_4 \end{Bmatrix}$$
$$S = 2(j_1^- + j_2^-) + (j_3^- - j_3^+ + j_3) + (j_4^- - j_4^+ + j_4) = 2(j_1^- + j_2^-) + S_3 + S_4 \tag{A.11}$$

The following identities are particularly useful in the calculation of spin foam amplitudes:

$$\mathcal{K}^{0\, J_1 J_2 J_3}(l, \beta) \equiv \mathcal{K}^{J_1 J_2 J_3}(l, \beta) = \sum_{j_1 j_2 j_3} \prod_{i=1}^{3} d_{j_i} w^l(J_i, j_i, \beta) \begin{Bmatrix} j_1^- & j_2^- & j_3^- \\ j_1^+ & j_2^+ & j_3^+ \\ j_1 & j_2 & j_3 \end{Bmatrix}^2 \tag{A.12}$$

$$\mathcal{K}^{j^- j^+}(l, \beta) = \sum_{j_1 j_2 j_3} \prod_{i=1}^{3} d_{j_i} w^l(j^-, j^+, j_i, \beta) \begin{Bmatrix} j^- & j^- & j^- \\ j^+ & j^+ & j^+ \\ j_1 & j_2 & j_3 \end{Bmatrix}^2 \tag{A.13}$$

These formula are completely general. For the (euclidean) EPRL model we have:

$$\mathcal{K}^{J_1 J_2 J_3}_{\mathrm{EPRL}}(\beta) = \prod_{i=1}^{3} \delta_{j_i^- |\beta| j_i^+} d_{(1-\beta) j_i^+} \begin{Bmatrix} |\beta| j_1^+ & |\beta| j_2^+ & |\beta| j_3^+ \\ j_1^+ & j_2^+ & j_3^+ \\ (1-\beta) j_1^+ & (1-\beta) j_2^+ & (1-\beta) j_3^+ \end{Bmatrix}^2 \tag{A.14}$$

$$\mathcal{K}^{j^- j^+}(\beta < 0) = \left[\frac{4a}{3\pi b}\right]^{\frac{1}{2}} \frac{\delta_{j^- |\beta| j^+}(1+3aj^+)}{\sqrt{j^+}(1+3j^+)(1+3bj^+)} \underset{j \to +\infty}{\approx} \frac{\delta_{j^- |\beta| j^+}}{(j^+)^{\frac{3}{2}}} \tag{A.15}$$

$$\mathcal{K}^{j^- j^+}(\beta \geq 0) = \left[\frac{4}{3\pi\delta b}\right]^{\frac{1}{2}} \delta_{j^- |\beta| j^+} \frac{(1+3j^+)(1+3\delta j^+)^2}{\sqrt{j^+}(1+3bj^+)(1+2j^+)^3} \underset{j \to +\infty}{\approx} \frac{\delta_{j^- |\beta| j^+}}{(j^+)^{\frac{3}{2}}} \tag{A.16}$$

where we have used the identities A.13, A.6 and A.7 together with the EPRL simplicity constraints.

B Elements of graph theory.

We collect here few elementary graph-theoretic notions often mentioned in the analysis of radiative corrections.

Contractible face - An (internal) face f of a GFT graph $\mathcal{G}$ is contractible if it has at least one edge e which is not shared with any other internal face of the same graph.

Contractible graph - A GFT graph $\mathcal{G}$ is contractible if its bulk holonomies h_{ve} can be trivialized in the UV region. A 1PI divergent contractible graph generate a counterterm proportional to a tensor invariant effective interaction (not necessarely a connected bubble.)

Tracial graph - A tracial GFT graph $\mathcal{G}$ is a contractible graph which generates a connected tensor invariant bubble interaction. All melonic graphs are by construction tracial.

References

[1] D. Oriti, *The microscopic dynamics of quantum space as a group field theory*, in *Proceedings, Foundations of Space and Time: Reflections on Quantum Gravity: Cape Town, South Africa*, pp. 257–320, 2011, 1110.5606.

[2] T. Krajewski, *Group field theories*, *PoS* **QGQGS2011** (2011) 005 [1210.6257].

[3] D. Oriti, *Group Field Theory and Loop Quantum Gravity*, 2014, 1408.7112.

[4] R. Gurau and J. P. Ryan, *Colored Tensor Models - a Review*, *SIGMA* **8** (2012) 020 [1109.4812].

[5] V. Rivasseau, *The Tensor Track, III*, *Fortsch. Phys.* **62** (2014) 81 [1311.1461].

[6] R. Gurau, *Notes on Tensor Models and Tensor Field Theories*, 1907.03531.

[7] S. Carrozza, *Tensorial methods and renormalization in Group Field Theories*, Ph.D. thesis, Orsay, LPT, 2013. 1310.3736. 10.1007/978-3-319-05867-2.

[8] S. Carrozza, *Flowing in Group Field Theory Space: a Review*, *SIGMA* **12** (2016) 070 [1603.01902].

[9] N. Bodendorfer, *An elementary introduction to loop quantum gravity*, 1607.05129.

[10] D. Oriti, *Group field theory as the 2nd quantization of Loop Quantum Gravity*, *Class. Quant. Grav.* **33** (2016) 085005 [1310.7786].

[11] A. Baratin and D. Oriti, *Group field theory and simplicial gravity path integrals: A model for Holst-Plebanski gravity*, *Phys. Rev.* **D85** (2012) 044003 [1111.5842].

[12] M. Finocchiaro and D. Oriti, *Spin foam models and the Duflo map*, *Class. Quant. Grav.* **37** (2020) 015010 [1812.03550].

[13] A. Perez, *The Spin-Foam Approach to Quantum Gravity*, *Living Rev. Relativity* **16** (2013) 3 [1205.2019].

[14] M. Dupuis, J. P. Ryan and S. Speziale, *Discrete gravity models and Loop Quantum Gravity: a short review*, *SIGMA* **8** (2012) 052 [1204.5394].

[15] J. C. Baez and J. W. Barrett, *The Quantum tetrahedron in three-dimensions and four-dimensions*, *Adv. Theor. Math. Phys.* **3** (1999) 815 [gr-qc/9903060].

[16] L. Freidel and S. Speziale, *Twisted geometries: A geometric parametrisation of SU(2) phase space*, *Phys. Rev.* **D82** (2010) 084040 [1001.2748].

[17] L. Freidel and E. R. Livine, *Bubble networks: framed discrete geometry for quantum gravity*, *Gen. Rel. Grav.* **51** (2019) 9 [1810.09364].

[18] L. Freidel, E. R. Livine and D. Pranzetti, *Gravitational edge modes: from Kac–Moody charges to Poincaré networks*, *Class. Quant. Grav.* **36** (2019) 195014 [1906.07876].

[19] M. Dupuis and E. R. Livine, *Lifting SU(2) Spin Networks to Projected Spin Networks*, *Phys. Rev.* **D82** (2010) 064044 [1008.4093].

[20] E. Baloitcha, V. Lahoche and D. Ousmane Samary, *Flowing in discrete gravity models and Ward identities: A review*, 2001.02631.

[21] A. Perez, *On the regularization ambiguities in loop quantum gravity*, *Phys. Rev.* **D73** (2006) 044007 [gr-qc/0509118].

[22] V. Bonzom and M. Smerlak, *Bubble divergences: sorting out topology from cell structure*, *Annales Henri Poincare* **13** (2012) 185 [1103.3961].

[23] J. Ben Geloun and V. Bonzom, *Radiative corrections in the Boulatov-Ooguri tensor model: The 2-point function*, *Int. J. Theor. Phys.* **50** (2011) 2819 [1101.4294].

[24] J. Ben Geloun, *On the finite amplitudes for open graphs in Abelian dynamical colored Boulatov–Ooguri models*, *J. Phys.* **A46** (2013) 402002 [1307.8299].

[25] C. Perini, C. Rovelli and S. Speziale, *Self-energy and vertex radiative corrections in LQG*, *Phys. Lett.* **B682** (2009) 78 [0810.1714].

[26] J. Ben Geloun, R. Gurau and V. Rivasseau, *EPRL/FK Group Field Theory*, *EPL* **92** (2010) 60008 [1008.0354].

[27] V. Bonzom and B. Dittrich, *Bubble divergences and gauge symmetries in spin foams*, *Phys. Rev.* **D88** (2013) 124021 [1304.6632].

[28] A. Riello, *Self-energy of the Lorentzian Engle-Pereira-Rovelli-Livine and Freidel-Krasnov model of quantum gravity*, *Phys. Rev.* **D88** (2013) 024011 [1302.1781].

[29] L.-Q. Chen, *Bulk amplitude and degree of divergence in 4d spin foams*, *Phys. Rev.* **D94** (2016) 104025 [1602.01825].

[30] P. Donà, *Infrared divergences in the EPRL-FK Spin Foam model*, *Class. Quant. Grav.* **35** (2018) 175019 [1803.00835].

[31] P. Dona and G. Sarno, *Numerical methods for EPRL spin foam transition amplitudes and Lorentzian recoupling theory*, *Gen. Rel. Grav.* **50** (2018) 127 [1807.03066].

[32] P. Donà, F. Gozzini and G. Sarno, *Searching for classical geometries in spin foam amplitudes: a numerical method*, 1909.07832.

[33] P. Donà, M. Fanizza, G. Sarno and S. Speziale, *Numerical study of the Lorentzian Engle-Pereira-Rovelli-Livine spin foam amplitude*, *Phys. Rev.* **D100** (2019) 106003 [1903.12624].

[34] S. Carrozza, V. Lahoche and D. Oriti, *Renormalizable Group Field Theory beyond melonic diagrams: an example in rank four*, *Phys. Rev.* **D96** (2017) 066007 [1703.06729].

[35] D. Oriti, *Group field theory as the microscopic description of the quantum spacetime fluid: A New perspective on the continuum in quantum gravity*, *PoS* **QG-PH** (2007) 030 [0710.3276].

[36] D. Oriti, *The Bronstein hypercube of quantum gravity*, 2018. 1803.02577.

[37] B. Dittrich, *The continuum limit of loop quantum gravity - a framework for solving the theory*, in *Loop Quantum Gravity: The First 30 Years* (A. Ashtekar and J. Pullin, eds.), pp. 153–179. 2017. 1409.1450. DOI.

[38] C. Delcamp and B. Dittrich, *Towards a phase diagram for spin foams*, *Class. Quant. Grav.* **34** (2017) 225006.

[39] A. Eichhorn, T. Koslowski and A. D. Pereira, *Status of background-independent coarse-graining in tensor models for quantum gravity*, *Universe* **5** (2019) 53 [1811.12909].

[40] A. Eichhorn, J. Lumma, A. D. Pereira and A. Sikandar, *Universal critical behavior in tensor models for four-dimensional quantum gravity*, *JHEP* **02** (2020) 110 [1912.05314].

[41] L. Freidel and D. Louapre, *Nonperturbative summation over 3-D discrete topologies*, *Phys. Rev.* **D68** (2003) 104004 [hep-th/0211026].

[42] J. Magnen, K. Noui, V. Rivasseau and M. Smerlak, *Scaling behaviour of three-dimensional group field theory*, *Class. Quant. Grav.* **26** (2009) 185012 [0906.5477].

[43] A. Baratin, S. Carrozza, D. Oriti, J. Ryan and M. Smerlak, *Melonic phase transition in group field theory*, *Lett. Math. Phys.* **104** (2014) 1003 [1307.5026].

[44] S. Carrozza and V. Lahoche, *Asymptotic safety in three-dimensional SU(2) Group Field Theory: evidence in the local potential approximation*, *Class. Quant. Grav.* **34** (2017) 115004 [1612.02452].

[45] J. Ben Geloun, T. A. Koslowski, D. Oriti and A. D. Pereira, *Functional Renormalization Group analysis of rank 3 tensorial group field theory: The full quartic invariant truncation*, *Phys. Rev.* **D97** (2018) 126018 [1805.01619].

[46] J. Ben Geloun, R. Martini and D. Oriti, *Functional Renormalisation Group analysis of Tensorial Group Field Theories on $\mathbb{R}^d$*, *Phys. Rev.* **D94** (2016) 024017 [1601.08211].

[47] D. Oriti, L. Sindoni and E. Wilson-Ewing, *Emergent Friedmann dynamics with a quantum bounce from quantum gravity condensates*, *Class. Quant. Grav.* **33** (2016) 224001 [1602.05881].

[48] S. Gielen and L. Sindoni, *Quantum Cosmology from Group Field Theory Condensates: a Review*, *SIGMA* **12** (2016) 082 [1602.08104].

[49] D. Oriti, *The universe as a quantum gravity condensate*, *Comptes Rendus Physique* **18** (2017) 235 [1612.09521].

[50] M. Finocchiaro, *Radiative corrections in GFT models for Quantum Gravity*, *To appear* .

[51] M. Celoria, M. Finocchiaro and D. Oriti, *Numerical analysis of the fusion coefficients of the Duflo spin foam model for 4d Riemannian quantum gravity*, *To appear* .

[52] V. Bonzom and M. Smerlak, *Gauge symmetries in spinfoam gravity: the case for 'cellular quantization'*, *Phys. Rev. Lett.* **108** (2012) 241303 [1201.4996].

[53] A. Kegeles and D. Oriti, *Continuous point symmetries in Group Field Theories*, *J. Phys.* **A50** (2017) 125402 [1608.00296].

[54] R. Gurau, *A generalization of the Virasoro algebra to arbitrary dimensions*, *Nucl. Phys.* **B852** (2011) 592 [1105.6072].

[55] N. Delporte and V. Rivasseau, *The Tensor Track V: Holographic Tensors*, in *Proceedings, 17th Hellenic School and Workshops on Elementary Particle Physics and Gravity (CORFU2017): Corfu, Greece, September 2-28, 2017*, 2018, 1804.11101.

[56] Y. Li, D. Oriti and M. Zhang, *Group field theory for quantum gravity minimally coupled to a scalar field*, *Class. Quant. Grav.* **34** (2017) 195001 [1701.08719].

[57] E. Wilson-Ewing, *A relational Hamiltonian for group field theory*, *Phys. Rev.* **D99** (2019) 086017 [1810.01259].

[58] S. Gielen and D. Oriti, *Cosmological perturbations from full quantum gravity*, *Phys. Rev. D* **98** (2018) 106019 [1709.01095].

[59] B. Dittrich, E. Schnetter, C. J. Seth and S. Steinhaus, *Coarse graining flow of spin foam intertwiners*, *Phys. Rev.* **D94** (2016) 124050 [1609.02429].

[60] B. Bahr and S. Steinhaus, *Hypercuboidal renormalization in spin foam quantum gravity*, *Phys. Rev.* **D95** (2017) 126006 [1701.02311].

[61] B. Bahr, *On background-independent renormalization of spin foam models*, *Class. Quant. Grav.* **34** (2017) 075001 [1407.7746].

[62] B. Dittrich, S. Mizera and S. Steinhaus, *Decorated tensor network renormalization for lattice gauge theories and spin foam models*, *New J. Phys.* **18** (2016) 053009 [1409.2407].

[63] W. J. Cunningham, B. Dittrich and S. Steinhaus, *Tensor network renormalization with fusion charges: applications to 3d lattice gauge theory*, 2002.10472.

[64] G. Vidal, *Entanglement Renormalization*, *Phys. Rev. Lett.* **99** (2007) 220405 [cond-mat/0512165].

[65] R. Orus, *A Practical Introduction to Tensor Networks: Matrix Product States and Projected Entangled Pair States*, *Annals Phys.* **349** (2014) 117 [1306.2164].

[66] G. Chirco, D. Oriti and M. Zhang, *Group field theory and tensor networks: towards a Ryu–Takayanagi formula in full quantum gravity*, *Class. Quant. Grav.* **35** (2018) 115011 [1701.01383].

[67] Q. Hu, A. Franco-Rubio and G. Vidal, *Continuous tensor network renormalization for quantum fields*, 1809.05176.

[68] L. Tagliacozzo, A. Celi and M. Lewenstein, *Tensor Networks for Lattice Gauge Theories with continuous groups*, *Phys. Rev.* **X4** (2014) 041024 [1405.4811].

[69] D. A. Varshalovich, A. N. Moskalev and V. K. Khersonsky, *Quantum Theory of Angular Momentum: Irreducible Tensors, Spherical Harmonics, Vector Coupling Coefficients, 3nj Symbols*. World Scientific, Singapore, 1988, 10.1142/0270.